Optimizing the Carbonic Anhydrase temperature response and stomatal conductance of carbonyl sulfide leaf uptake in the simple biosphere model (SiB4)

Ara Cho[1], Linda M.J. Kooijmans[1], Kukka-Maaria Kohonen[2], Richard Wehr[3], Maarten C. Krol[1,4]

[1]Meteorology and Air Quality, Wageningen University and Research Centre, Wageningen, The Netherlands
[2]Institute for Atmospheric and Earth System Research/ Physics, Faculty of Science, University of Helsinki, Helsinki, Finland
[3]Center for Atmospheric and Environmental Chemistry, Aerodyne Research, Inc., Billerica, MA, USA
[4]Institute for Marine and Atmospheric Research, Utrecht University, Utrecht, The Netherlands

Correspondence to: Ara Cho (ara.cho@wur.nl)

Abstract. Carbonyl Sulfide (COS) is a useful tracer to estimate Gross Primary Production (GPP) because it shares part of the uptake pathway with CO_2. COS is taken up in plants through hydrolysis, catalyzed by the enzyme carbonic anhydrase (CA), but is not released. The Simple Biosphere model version 4 (SiB4) simulates COS leaf uptake using a conductance approach. SiB4 applies the temperature response of the RuBisCo enzyme (used for photosynthesis) to simulate the COS leaf uptake, but the CA enzyme might respond differently. We introduce a new temperature response function for CA in SiB4, based on enzyme kinetics with an optimum temperature. Moreover, we determine Ball-Berry model parameters for stomatal conductance (g_s) using observation-based estimates of COS flux, GPP, and g_s along with meteorological measurements in an evergreen needleleaf forest (ENF) and deciduous broadleaf forest (DBF). We find that CA has optimum temperatures of 22 °C (ENF) and 38 °C (DBF) with CA's activation energy as 40 kJ mol^{-1}, which is lower than that of RuBisCo (45 °C), suggesting that air temperature changes can critically affect CA's catalyzation activity. Optimized values for the Ball-Berry offset parameter b_0 (ENF: 0.013, DBF: 0.007 mol m^{-2} s^{-1}) are higher (lower) than the original value (0.010 mol m^{-2} s^{-1}) in the ENF (DBF), and optimized values for the Ball-Berry slope parameter b_1 (ENF: 16.36, DBF: 11.43) are higher than the original value (9.0) at both sites. We apply the optimized g_{CA} and g_s parameters in SiB4 site simulations, thereby improving the timing and peak of COS assimilation. In addition, we show that SiB4 underestimates the leaf humidity stress under conditions where high VPD should limit g_s in the afternoon, thereby overestimating g_s. Furthermore, we simulate global COS biosphere fluxes, which show smaller COS uptake in the tropics and larger COS uptake at higher latitudes, corresponding with the updates made to the CA temperature response. This SiB4 update helps resolve gaps in the COS budget identified in earlier studies. Using our optimization and additional observations of COS uptake over various climate and plant types, we expect further improvements in global COS biosphere flux estimates.

1 Introduction

The leaf assimilation of the atmospheric trace gas carbonyl sulfide (COS) has been suggested as a proxy to overcome the limitations of estimating photosynthetic carbon dioxide (CO_2) assimilation (Whelan et al., 2018). Observations of the net ecosystem exchange (NEE) of CO_2 include both Gross Primary Production (GPP) and ecosystem respiration, and those two individual components cannot be directly observed. COS follows the same diffusional pathway into leaves through plant stomata as CO_2. COS is then destroyed through hydrolysis catalyzed by the enzyme carbonic anhydrase (CA) and is assumed not to be produced by any process within leaves (Protoschill-Krebs et al., 1996; Stimler et al., 2010). The CA chemistry is not light-dependent (Protoschill-Krebs et al., 1996), in contrast to photosynthetic CO_2 fixation, which requires light. Therefore, measurements of COS uptake can provide information on stomatal conductance, e.g. during the night (Kooijmans et al., 2017), which cannot be obtained from CO_2 measurements.

Atmospheric COS mole fractions vary around 500 parts per trillion (ppt) and are primarily influenced by biosphere uptake, ocean emissions, and anthropogenic emissions (Kettle et al., 2002). Recent studies have found that a source is missing in the tropical region (Berry et al., 2013; Glatthor et al., 2015; Kuai et al., 2015; Ma et al., 2021). Moreover, Berry et al. (2013) showed that a sink is missing, or a source is overestimated at higher latitudes. These findings ask for careful evaluation of all sources and sinks, including the biosphere.

Biosphere models, such as the Simple Biosphere model, version 4 (SiB4) (Berry et al., 2013; Kooijmans et al., 2021) and the Organizing Carbon and Hydrology In Dynamic Ecosystems model (ORCHIDEE; Launois et al., 2015; Maignan et al., 2021, Remaud et al., 2021, Abadie et al., 2021) have been used to estimate ecosystem exchange of COS quantitatively. The SiB4 COS biosphere exchange was recently assessed against observations by Kooijmans et al. (2021). They stressed the need to account for spatial and temporal variations in atmospheric COS mole fractions, which largely reduce SiB4 COS biosphere uptake in the tropics (although observations to confirm this influence are lacking). The calculated reduction in the tropics was not large enough to explain the gap in the COS budget. Kooijmans et al. (2021) and Vesala et al., (2022) also found that SiB4 COS biosphere flux simulations were low compared to observations in the boreal region, consistent with the underestimations found by Ma et al. (2021). Our study follows one of the recommendations in Kooijmans et al. (2021) by focusing on the parameterization of the temperature dependence of the CA enzyme activity to improve simulations of the vegetation COS uptake in SiB4.

In SiB4, the COS assimilation is described as a series of resistances (i.e. inverse conductances) at the leaf boundary layer (g_b), the stomatal pores (g_s), and the leaves' interior (g_{CA}). These conductances to COS are scaled relative to conductances for water vapor or CO_2 with diffusivity ratios and a calibration factor. For g_{CA}, previous studies found that both the CA enzyme activity (Badger and Price 1994) and mesophyll conductance (Evans et al., 1994) scale with the maximum velocity of carboxylation

(V_{max}) by the enzyme RuBisCo. Therefore, the COS internal conductance in SiB4 is scaled to V_{max} through a single calibration factor α based on laboratory leaf gas exchange measurements (Stimler et al., 2010, 2011, Berry et al., 2013). However, the

65   enzymatic control of COS and CO_2 assimilation differ. COS molecules are hydrolyzed by the enzyme CA in the mesophyll cells (Protoschill-Kreb et al., 1996). In contrast, photosynthesis is further controlled by the enzyme RuBisCo. Thus, CO_2 has a different point of uptake compared to COS. The enzyme activity depends on the enzyme abundance and is related to environmental parameters such as temperature and pH (Michaelis and Menten, 1913). In particular, the CA enzyme does not require light to catalyze COS hydrolysis, whereas the RuBisCo enzyme does require light (Stimler et al., 2010).

70

Several studies found that the leaf relative uptake ratio (LRU, which is proportional to the ratio of COS and CO_2 deposition velocities) varies with temperature under conditions where light was not limiting photosynthesis (Cochavi et al., 2021; Stimler et al., 2010; Sun et al., 2018; Kooijmans et al., 2019). More specifically, the LRU decreased with increasing temperatures above 15 ℃, indicating that COS uptake has a lower optimum temperature than CO_2 uptake, possibly driven by different

75   temperature responses of the CA and RuBisCo enzymes. Therefore, to accurately simulate the relation between COS and CO_2 exchange in leaves, it is necessary to use separate temperature response equations for the internal conductance to CO_2 and COS.

Besides uncertainties in g_{CA}, uncertainties in g_s can also affect the accuracy of simulated COS assimilation. A common

80   approach for simulating g_s is the semi-empirical Ball-Berry (BB) model (e.g. Ball et al., 1987; Ball 1988; Collatz et al., 1992). This model is also applied in SiB4 and utilizes a set of related variables (e.g. relative humidity, CO_2 concentration at the leaf surface, photosynthesis) and two empirical constants. One of the constants (b_1) describes the slope of the relation between g_s and GPP. The other constant (b_0) represents the residual g_s in the dark. The current implementation of the BB model in SiB4 has only one pair of b_1 and b_0 values for C3 plants and only one pair for C4 plants, whereas the BB constants should ideally

85   be prescribed for each plant functional type (PFT) separately to obtain accurate g_s (Miner et al., 2017). To constrain b_0 requires information on nighttime g_s. However, obtaining g_s estimates from nighttime water vapor flux measurements in the field is highly uncertain due to observational constraints (Papale et al., 2006; Wehr et al., 2017; Wehr and Saleska, 2021). As an alternative, nighttime COS uptake was previously reported (White et al., 2010; Belviso et al., 2013; Commane et al., 2013, 2015; Berkelhammer et al., 2014; Billesbach et al., 2014; Wehr et al., 2017; Kooijmans et al., 2017), and when the soil uptake

90   is properly accounted for, this flux could provide information on stomatal opening. Several multi-year measurement datasets of CO_2 and COS biosphere and soil fluxes are now available (Commane et al., 2015; Wehr et al., 2017; Vesala et al., 2022), making it possible to use COS to provide information on g_s and thereby constrain the BB model parameters.

This research aims to optimize the temperature response of CA and BB model parameters to better estimate COS assimilation

95   in the SiB4 model. To do so, we will use observed COS leaf fluxes and GPP, plus observation-based g_s. The optimization will be based on observations from two PFTs: a boreal evergreen needleleaf forest (ENF) in Hyytiälä, Finland and a temperate

deciduous broadleaf forest (DBF) at Harvard Forest, USA. The optimized parameters will be applied in the global simulation of the SiB4 biosphere model to evaluate the effects on the global COS biosphere sink.

2 Methodology

2.1 Modelling COS leaf uptake

2.1.1 SiB4 biosphere model

The SiB4 model is a land surface model that calculates the COS flux as described in Berry et al. (2013). The main application of the model is to estimate land-atmosphere exchange of carbon, land surface energy, and water budgets (Sellers et al., 1986; Sato et al., 1989). SiB4 has a timestep of 10-minutes and operates on a spatial resolution of 0.5° x 0.5°. Unlike the previous SiB3 model, which relies on satellite information, version 4 fully simulates the terrestrial carbon cycle using a process-based model (Haynes et al., 2019).

As each vegetation type has different physiological and phenological characteristics, SiB4 simulates photosynthesis in a heterogenic land cover with different plant functional types (PFTs) per site or grid cell, each with separate fractions. These PFTs consist of nine natural vegetation classes and three specific crop types (maize, soybeans, and winter wheat), plus the separation of C3 and C4 plants in generic cropland and grassland. Besides responses of plant growth to temperature, humidity, radiation, and precipitation, the model accounts for environmental stress factors as a limitation to plant growth: the leaf humidity stress (F_{LH}), the root-zone water stress (F_{RZ}), and the canopy temperature stress (F_T). Several variables (e.g. V_{max} of RuBisCo) are prescribed according to phenological stages: leaf-out, growth, maturity, senescence, and dormant stages. The leaf-out stage begins when the environmental conditions are suitable for photosynthesis to take place, and the growth stage is determined when the canopy is large enough to support photosynthesis. The maturity starts when the leaf amount is maintained. When plants experience stress and photosynthetic capacity is reduced, it is prescribed as senescence. In the dormant stage, plants do not have leaves in the canopy, or it has unsuitable conditions for photosynthesis (Haynes et al., 2020).

2.1.2 Module for COS vegetation uptake in SiB4

SiB4 simulates COS vegetation assimilation as a combination of three resistances (g_s, g_b, and g_{CA}) multiplied by the atmospheric COS mole fraction (Berry et al., 2013):

$$F_{cos} = C_{cos} \left(\frac{1.94}{g_s} + \frac{1.56}{g_b} + \frac{1}{g_{CA}} \right)^{-1} \tag{1}$$

where F_{cos} is the COS vegetation assimilation in the canopy (pmol m^{-2} s^{-1}), and C_{cos} is the atmospheric COS mole fraction in the canopy (pmol mol^{-1}). Due to its larger size, COS diffusion through the stomata and the laminar boundary are slowed down by a factor of 1.94 and 1.56, respectively, relative to water vapor (Seibt et al., 2010; Stimler et al., 2010).

The stomatal conductance g_s (mol m^{-2} s^{-1}) in SiB4 is calculated by using the BB model. This model relates g_s and GPP as a function of environmental factors with two empirical constants b_0 and b_1:

$$g_s = b_1 \frac{GPP_{SiB4}}{CO_{2s}} F_{LH} + b_0 \cdot LAI \cdot F_{RZ} \tag{2}$$

130 where GPP_{SiB4} (mol C m^{-2} s^{-1}) is the canopy CO$_2$ assimilation, CO_{2S} (mol C mol air^{-1}) is the CO$_2$ mole fraction at the leaf surface, F_{LH} (-) is the leaf humidity stress factor, LAI is the leaf area index (-), and F_{RZ} is a non-dimensional term that accounts for root-zone water stress. F_{LH} is related to relative humidity at the leaf surface and is calculated as a ratio of the water vapor mixing ratio at the leaf surface to the water vapor mixing ratio in the leaf internal space (Sellers et al. 1992). The value of F_{LH} for ENF has a lower bound of 0.7, making ENF more resilient to humidity stress. However, Smith et al. (2020) found that with

135 the 0.7 threshold in place, SiB4 did not accurately simulate a drought response for European ENF ecosystems. Therefore, we removed this lower bound in the optimization, but will show the impact in a sensitivity study in Sect. 3.5.1.

The empirical constant b_1 is the slope of the linear relationship between g_s and GPP_{SiB4} F_{LH} $CO_{2s}$$^{-1}$ and b_0 (mol m^{-2} s^{-1}) is the intercept indicating minimum g_s (Ball et al., 1987; Ball 1988). The choice for b_1 significantly impacts simulated transpiration

140 (Leuning et al., 1998; Lai et al., 2000; Bauerle et al., 2014) and is prescribed in SiB4 as 9.0 for C3 plants and 4.0 for C4 plants. The coefficient b_0 is 0.01 mol m^{-2} s^{-1} for most PFTs but 0.04 mol m^{-2} s^{-1} for crops and C4 plants. The prescribed b_0 term is converted from the leaf to the canopy scale by multiplying by LAI.

GPP_{SiB4} is explicitly calculated in SiB4 using the carbon pool with three assimilation rates limited by enzyme activity (w_c),

145 light (w_e), and carbon compound export (w_s) (Haynes et al., 2020). The three rates are calculated by functions $f_{c,e,s}$ described in detail in Sellers et al. (1996) depending on a canopy temperature (T_{can}, K):

$$w_c = f_c(V_{max}(T_{can}), pCO_{2i}, pO_2(T_{can}), \gamma^*) \tag{3}$$
$$w_e = f_e(APAR, pCO2_i, \gamma^*) \tag{4}$$
$$w_s = f_s(V_{max}(T_{can}), F_{RZ}, pO_2(T_{can})) \tag{5}$$

150 Where pCO_{2i} (Pa) is the internal partial pressure of CO$_2$, $pO_2(T)$ (Pa) is the temperature response of partial pressure of O$_2$, APAR (mol m^{-2} s^{-1}) is the absorbed photosynthetically active radiation, and γ^* (Pa) is the CO$_2$ photo-compensation point. The SiB4 model defines GPP as the minimum of these three limiting rates. Note that GPP_{SiB4} is used in SiB4 to calculate the COS leaf flux via g_s, as described in Eq. (2) and evaluated independently from GPP calculated by the BB model (GPP_{BB}) which will be introduced in Sect. 2.3.1.

155

The COS molecules that have diffused into the leaf mesophyll cells are hydrolyzed in a reaction catalyzed by the CA enzyme (g_{CA}). SiB4 assumes that the g_{CA} (mol m^{-2} s^{-1}) scales with V_{max} of RuBisCo at 298 K ($V_{max, rub}$, mol m^{-2} s^{-1}) as follows:

$$g_{CA}(PS) = \alpha \cdot V_{max,rub}(PS) \cdot f(T_{can})_{SiB4} \cdot F_{LC}(PS) \cdot F_{RZ} \cdot \left(\frac{P}{P_{sfc}}\right) \cdot \left(\frac{T_{can}}{T_0}\right) \tag{6}$$

$V_{max, rub}$ varies with phenological stage (PS) (see Table 3) and is scaled with a T_{can} response function $f(T_{can})_{SiB4}$ that prescribes

160   the relative increase per 10 K increase (Q_{10}) as 2.1:

$$f(T_{can})_{SiB4} = 2.1^{0.1(T_{can}-298)} \qquad (7)$$

In SiB4, the canopy temperature T_{can} is calculated from the temperature above the canopy, which is normally obtained from a meteorological analysis dataset (Haynes et al., 2020). In this study, however, we use the temperature measured above the canopy to obtain T_{can} by SiB4. Likewise, we use the specific humidity measured above the canopy, which is used by SiB4 to

165   calculate the leaf humidity stress factor F_{LH} at leaf surface level, needed in Eq. (2).

Other modifying factors in Eq. (6) are the ratio of atmosphere pressure (P, hPa) to the surface pressure (P_{sfc} = 1,000 hPa) and the ratio of the temperature to the reference temperature (T_0 = 273.15 K). F_{LC} (-) is the scaling factor from leaf to canopy, accounting for a fraction of absorbed PAR (FPAR) and other factors such as light scattering and leaf projection. The calibration

170   parameter α (-) was obtained from simultaneous measurements of COS and CO_2 uptake (Stimler et al., 2010, 2012; Berry et al., 2013) and was estimated as 1400 for C3 and 8862 for C4 plants. These numbers were derived from a limited number of observations, so the values of α do not capture variability between plant species and seasons. Kooijmans et al. (2021) derived α from ecosystem observations of six sites throughout the growing season and found an average α of 1616 ± 562 (C3 plants). Here, the standard deviation indicates large variability over time and between sites. The impact of α on g_{CA} will be described

175   in Sect. 2.1.3.

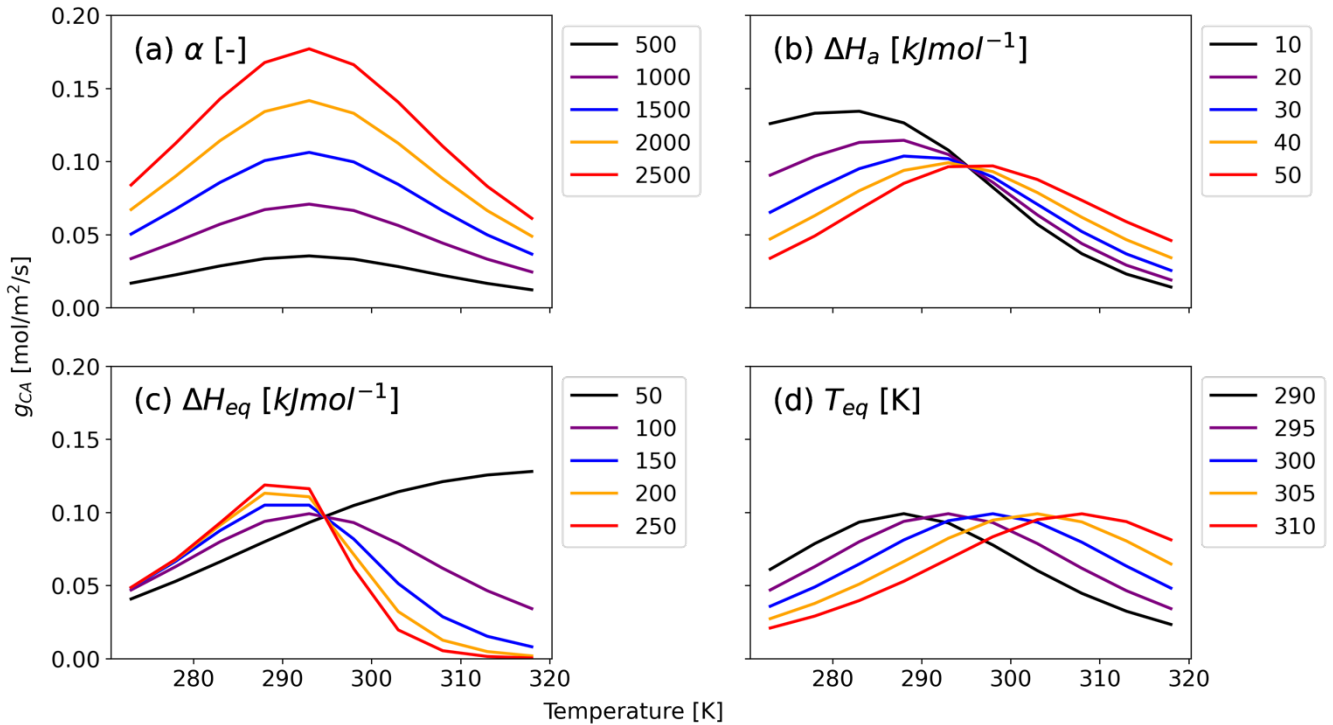### 2.1.3 A new approach to describe g_{CA}

Each enzyme has its own kinetic characteristics, with activity generally increasing with temperature up to an optimum temperature and decreasing above this temperature. To derive a more realistic enzyme activity that also accounts for an optimum temperature, we propose a temperature response ($f(T_{can})_{new}$) based on an equilibrium model that applies Michaelis-

180   Menten kinetics. A similar equilibrium model was previously used in COS soil models (Sun et al., 2015; Ogée et al., 2016) and is described as (Peterson et al. 2004; Daniel et al., 2010):

$$f(T_{can})_{new} = A_T \cdot \frac{T_{can}\exp\left(-\frac{\Delta H_a}{RT_{can}}\right)}{1+\exp\left[-\frac{\Delta H_{eq}}{R}\left(\frac{1}{T_{can}}-\frac{1}{T_{eq}}\right)\right]} \qquad (8)$$

Here, three variables for enzyme kinetics are included: ΔH_a (kJ mol^{-1}) is the activation free energy of the CA enzyme; ΔH_{eq} (kJ mol^{-1}) is the enthalpy change when the enzyme converts from an activated to inactivated state; T_{eq} (K) is the temperature

185   at which activated and inactive enzymes' concentrations are equal (Daniel et al., 2010; Sun et al., 2015). The factor A_T normalizes Eq. (8) such that, equivalent to Eq. (7), $f(T_{can})_{new}=1$ at $T_{can} = 298$ K. We adopt A_T as the value of $f(T_{can})_{new}{}^{-1}$ when T is equal to T_{eq}. R is the universal gas constant (8.3145 J K^{-1} mol^{-1}). Figure 1 shows that α and the three kinetic parameters have different effects on the temperature response of g_{CA} (Eq. 6). The calibration parameter α affects the strength of g_{CA} (Fig. 1(a)) and its accuracy is therefore crucial for accurate COS flux simulations. With ΔH_a increasing (Fig. 1(b)), g_{CA} decreases

(increases) for temperatures above (below) the optimal temperature. ΔH_{eq} has the opposite effect, albeit with a different response to ΔH_a (Fig. 1(c)). Both ΔH_a and ΔH_{eq} affect g_{CA} depending on the temperature range. Finally, Fig. 1(d) shows that T_{eq} determines the optimum of the temperature response curve without having impact on the magnitude of g_{CA}.

Figure 1: Calculated g_{CA} as a function of canopy temperature for parameters (a) α, (b) ΔH_a, (c) ΔH_{eq}, and (d) T_{eq} from Eq. (6), (8). Each parameter is set to five different values given in the caption to investigate the response of g_{CA} to temperature. While the target parameter changes, the other variables are fixed as $\alpha = 1400$ $\Delta H_a = 40$ kJ mol^{-1} $\Delta H_{eq} = 100$ kJ mol^{-1}, and $T_{eq} = 295$ K which are initial values for Hyytiälä (see Sect. 2.3.2).
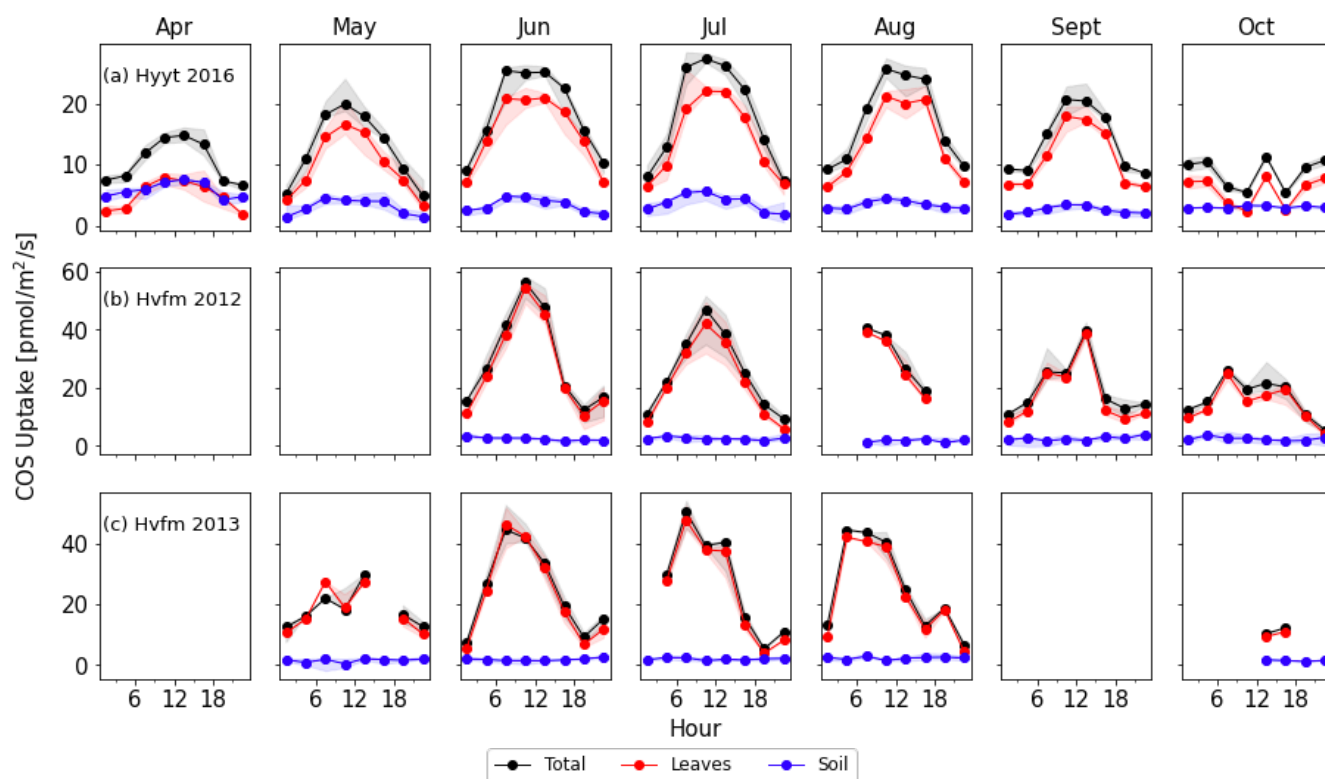
2.2 Observation

2.2.1 Observed variables

In the optimization of g_s and g_{CA}, we used observed values of the variables required in the COS leaf uptake calculation (Eq. (1)), namely: COS ecosystem flux, COS soil flux, GPP, C_{cos}, temperature, and specific humidity. The observations were obtained at Hyytiälä in Finland during 2013-2017 (Kooijmans et al., 2017; Sun et al., 2018; Vesala et al., 2022) and at the Harvard Forest in the United States during 2012 and 2013 (Commane et al., 2015; Commane et al., 2016; Wehr et al., 2017). COS and GPP ecosystem fluxes were measured with the eddy-covariance (EC) technique.

For Hyytiälä, the EC processing steps were described by Kohonen et al. (2020) and Vesala et al. (2022) and GPP was derived from NEE using multi-year parameter fits (Kolari et al., 2014, Kohonen et al., 2022). The effect of storage in the canopy

210 airspace was corrected by collocated COS profiles (Kooijmans et al., 2017; Kohonen et al., 2020).

For the Harvard Forest, we used GPP derived from CO_2 isotope EC measurements as reported in Wehr et al. (2016), and we used canopy COS uptake derived from COS EC measurements as reported in Wehr et al. (2017).

In addition to the COS ecosystem fluxes, COS soil flux measurements were available for the 2016 growing season at Hyytiälä, and for the 2012 and 2013 growing seasons the Harvard Forest.

215 To ensure data quality for the COS ecosystem flux, soil flux, GPP, and COS mole fraction, we used three-hourly averages each month for each observed variable. We removed outliers that fell out of the 25 to 75 percentile range in each three-hourly period. We only used data points when more than three data points were present at three-hourly time intervals in each month and when all variables required for the optimization were available.

220 Figure 2 shows the resulting average diurnal cycle per month for COS ecosystem, soil, and vegetation fluxes (ecosystem flux minus soil flux). Note that positive fluxes indicate uptake. As the seasonal and diurnal variations in COS soil fluxes were small (Sun et al., 2018), we applied the monthly average diurnal cycle of the soil flux from 2016 to the other years (2013-2015 and 2017).

Figure 2. Monthly diurnal variation of COS fluxes in 2016 at Hyytiälä (a) and 2012-2013 at Harvard Forest (b, c). Lines are median values, and filled areas show the 25 to 75 percentile range of the data. Black: COS ecosystem flux, blue: soil flux, red: vegetation flux estimated as ecosystem minus soil flux.

2.2.2 Observation-based g_s and g_{CA}

Observation-based g_s was derived from sensible heat flux and evapotranspiration measurements using the Flux Gradient (FG) equations (Baldocchi et al., 1991; Wehr and Saleska, 2015; Wehr and Saleska, 2021). A key step in the derivation of g_s is the estimation of transpiration from evapotranspiration. At the Harvard Forest, transpiration was estimated by an empirical equation established during times of minimal non-stomatal evaporation (i.e. a few days after rain, removing mornings with dew evaporation), as described in Wehr et al. (2017). At Hyytiälä, we simply restricted our analysis to periods of minimal non-stomatal evaporation by eliminating data when the dew point was equal to or greater than the air temperature or when the accumulated precipitation for the past two days was more than 0.01 mm.

The FG approach leads to significant uncertainties for nighttime data because the leaf to air-water vapor gradient is too small under stable conditions (Wehr et al., 2017). We thus excluded nighttime g_s when the values were smaller than 0.05 mol m^{-2} s^{-}

9

[1]. To reduce the effect of random noise on g_s, we used an average diurnal cycle (based on three-hourly medians) for each month.

245   Observation-based g_{CA} was extracted by rewriting Eq. (1):

$$g_{CA} = \left(\frac{C_{cos}}{F_{cos}} - \frac{1.94}{g_s} - \frac{1.56}{g_b} \right)^{-1} \tag{9}$$

Here we used the observation-based g_s from the FG equation as discussed above and filtered observations of C_{cos} and F_{cos}. Additionally, we used simulated g_b from SiB4, as we don't have observed g_b available and as the value of g_b only has a minor effect on F_{cos}, which will be further discussed in Sect. 3.1. Although outliers of observed g_s, C_{cos}, and F_{cos} were removed

250   already, a significant number of outliers in g_{CA} appeared because of error propagation. We removed additional outliers outside the 25–75 percentile range of the g_{CA} dataset.

2.3 Optimization

2.3.1 Procedure

In the optimization steps, we minimized a quadratic cost function $J(x)$ based on Bayes' theorem (Tarantola and Vallette 1982,

255   Enting et al., 1993):

$$J(x) = \frac{(x - x_a)^2}{2\sigma_a^2} + \frac{(y - H(x))^2}{2\sigma_y^2} \tag{10}$$

Here, x represents the state, x_a the prior settings of the state, and σ_a the error assigned to the parameters. In the second term, y represents the observations and $H(x)$ the model evaluation using the state x. The error σ_y represents the observational error. The details of σ_a and σ_y will be described in Sect. 2.3.2 and Sect. 2.3.3, respectively.

260

To optimize the g_s and g_{CA} parameters, we intend to use the information from GPP and COS leaf uptake measurements simultaneously. Thus, we propose a two-step approach in combination with an iterative minimization of the cost functions, as outlined in Fig. 3. In the first step, we optimally estimate g_s parameter b_1 by minimizing $J(x)$ which sums GPP differences between estimation ($H(b_1)$ in Eq. (10)) and observation. We select to use GPP observations in the optimization over g_s because

265   GPP can be used to evaluate b_1 and b_0 using the BB model. Moreover, observed GPP leads to more accurate b_1 values, because of uncertainties in GPP are smaller compared to observation-based g_s. Here, we use only positive GPP_{obs} values (uptake) because the BB model is only applicable in daytime conditions. The estimated GPP ($H(b_1)$ in Eq. (10)) is calculated by rewriting the BB model using observation-based g_s (Sect. 2.2.2), modelled RH at the leaf surface (F_{LH}), and simulated CO_{2S} from SiB4. Hereinafter the estimated GPP by the BB model is called GPP_{BB} :

270    $$GPP_{BB} = \frac{(g_s - b_0 \cdot LAI \cdot F_{RZ})\, CO_{2S}}{b_1 \cdot F_{LH}} \tag{11}$$

10

In the second optimization step, we optimize the b_0 and g_{CA} parameters (α in Eq. (6) and T_{eq} in Eq. (8)). These parameters are optimized by minimizing the differences between calculated and observed F_{COS}. F_{COS} is calculated with three conductances using Eq. (1). Specifically, g_s is estimated with Eq. (2) using the optimized b_1 from step 1. Here, we used GPP_{SiB4} to satisfy

275   our aim of optimizing the SiB4 model parameters. Note that GPP_{BB} from Eq. (11) cannot be used here, because it would make the estimated g_s equal to observation-based g_s. Based on sensitivity studies in Appendix A, we decided to select α, b_0, and T_{eq} as target parameters and to fix ΔH_{eq} and ΔH_a at 100 kJ mol^{-1} and 40 kJ mol^{-1}, respectively.

In the optimization procedure, we specifically exploit the fact that the nighttime COS flux carries information about nighttime

280   g_s through the parameter b_0. The alternative, i.e. optimizing b_0 already in step 1, would ignore the information of nighttime g_s brought by COS flux observations. Consequently, however, we have to iterate the procedure several times to reach convergence. Figure 3 specifies which observations are used in which step (g_s, GPP_{obs}, $F_{COS, obs}$, C_{cos} highlighted as grey) and which variables are simulated by SiB4 (e.g. T_{can}, F_{LH}, GPP_{SiB4}, CO_{2S}, g_b).
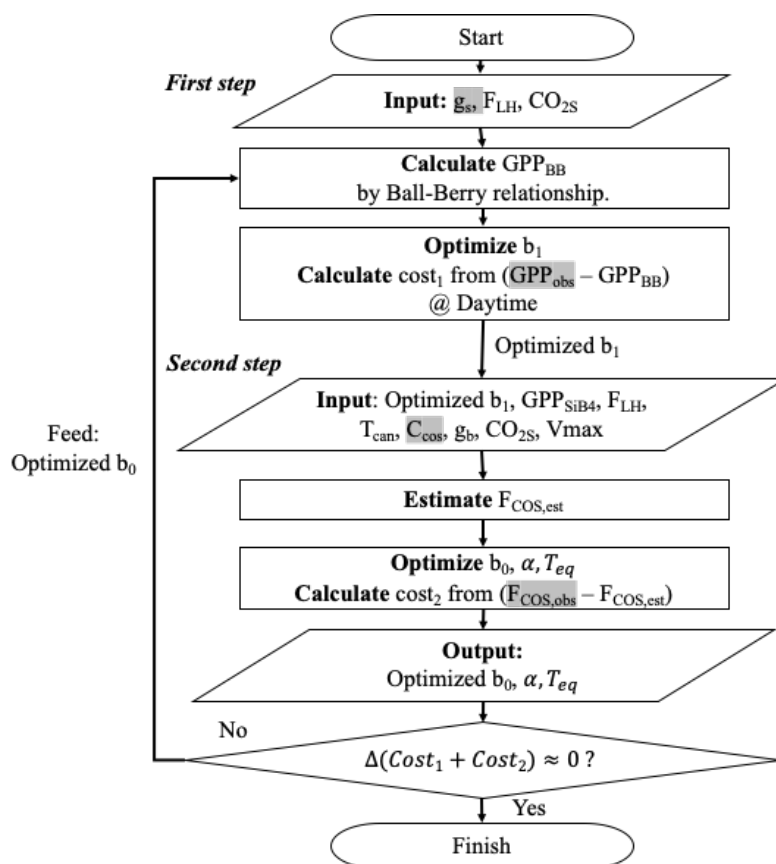
285   **Figure 3. Flow chart of the procedure to optimize COS leaf uptake's parameters. The procedure has two steps: (1) Optimize b_1 by minimizing deviations between GPP$_{BB}$ and observations, (2) Optimize b_0, α, and T_{eq} by minimizing deviations between modelled and observed COS uptake. Variables highlighted in grey are from observations, and the other variables are estimated from SiB4.**

We applied the Simplicial homology global optimization (SHGO) from the SciPy python library to minimize the cost functions.
290   SHGO is appropriate for solving non-continuous, non-convex and non-smooth functions (Endres et al., 2018). SHGO also
allows the definition of a valid parameter range, as will be discussed in Sect. 2.3.2 and in Appendix A.

The V_{max} of RuBisCo was found to vary over the phenological stage and per PFT (Woodward et al., 1995; Wolf et al., 2006;
Kattge et al., 2009; Walker et al., 2014), which also affects the calibration factor α. Therefore, we optimized α for each PFT
295   and each phenological stage. In contrast, b_0, b_1, and T_{eq} were only separately determined for the different PFTs, assuming local
characteristics for each PFT.

2.3.2 Initial parameters and prior errors

The first term in the cost function (Eq. (10)) ties the values of the parameters to realistic values. We additionally confined the
parameter values within realistic physical ranges using the SHGO algorithm. Initial parameters and prior errors were chosen
300   based on thresholds outlined in Appendix A, and they will be compared with optimized results in Sect. 3.3. The variation in
the resulting cost function shows distinct differences between Hyytiälä and Harvard Forest, which reinforces our strategy to
optimize parameters for each station separately.

2.3.3 Observation Errors

To quantify the observational errors σ_y, we first calculated the three-hourly average coefficient of variation (CV) relative to
305   the mean of the observed COS vegetation flux in each phenological stage and observed GPP for the entire growing season.
Figure 4 shows the results of observational errors. The GPP error is applied in step 1 and the COS leaf uptake error is used in
step 2 in the optimization. We multiplied the CV with the mean in each phenological stage. Here, we classify the error of the
COS leaf uptake in each phenological stage because we optimized α in each stage. In Fig. 4, we found that the errors differ
slightly per phenological stage. In Hyytiälä, the errors are larger in the growth stage compared to the maturity stage, possibly
310   due to the unstable weather conditions in growth stage. The COS leaf uptake error is larger at both stations during nighttime
than during daytime. A potential reason can be the relatively higher uncertainty in the eddy covariance method during stable
nighttime conditions.
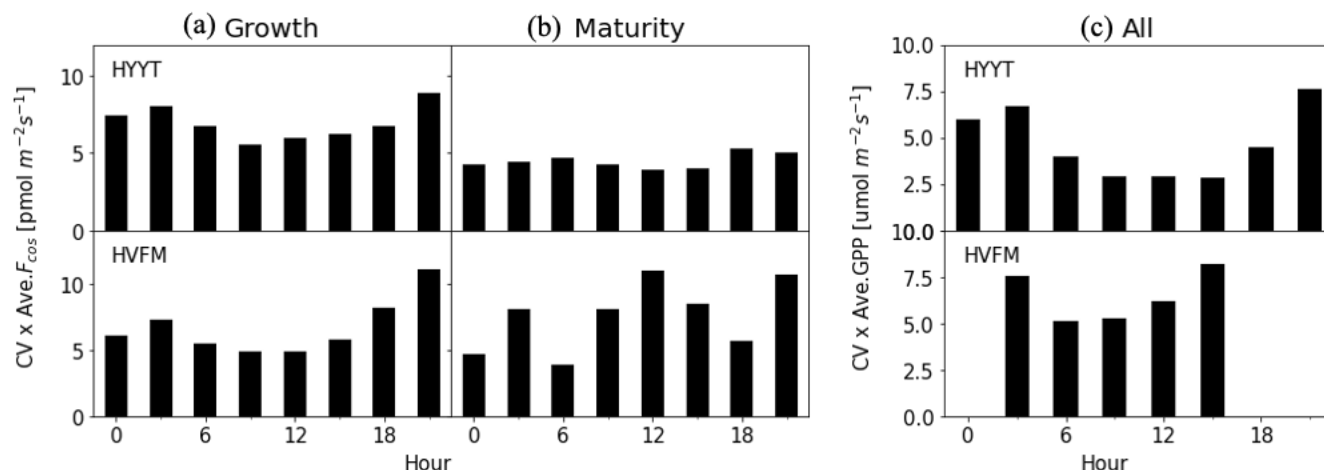
Figure 4. Distribution of the observation error in the growth (a) and maturity stages (b) for COS leaf uptake and all stages for GPP (c). The upper panel is the errors for Hyytiälä (HYYT) and the lower panel is for Harvard Forest (HVFM).

2.4 SiB4 simulations

We utilized several simulated variables from SiB4 in our optimization. Specifically, calculated GPP_{SiB4}, g_b, T_{can}, V_{max} of RuBisCo, functions F_{LH}, F_{RZ} and F_{LC} were used to calculate COS leaf uptake. In addition, LAI and CO_{2S} were used to estimate GPP_{BB}. Furthermore, we introduced the new temperature function ($f(T_{can})_{new}$) in the g_{CA} calculation (Sect. 2.2.3) to calculate COS leaf uptake, and excluded $P P_{sfc}^{-1}$ and $T_{can} T_0^{-1}$ from Eq. (3) due to minor impacts of these factors for these ecosystems.

To simulate the SiB4 data at the two stations, we used the Modern-Era Retrospective Analysis for Research and Application, version 2 (MERRA-2) (Gelaro et al., 2017) as meteorological driver data. Only air temperature and leaf specific humidity were taken from observations. To initialize the carbon pools, we spun up the model to equilibrate the pools. The spin-up was performed from 2000 to 2010 with ten iterations. Ambient CO_2 mole fractions were prescribed at 370 ppm.

To estimate the global impact of our findings, we performed a global simulation to evaluate COS leaf uptake estimated by the updated g_s and g_{CA} values. The atmospheric COS mixing ratio C_{cos} were taken from optimizations using the TM5 chemical transport model (Ma et al., 2021; Kooijmans et al., 2021). As we found that all target parameters differ per PFT in Sect. 2.3.2, we applied these parameters only to ENF and DBF. However, to confirm the $f(T_{can})_{new}$ effect on COS leaf uptake, we applied $f(T_{can})_{new}$ to all PFTs with averaged optimum T_{eq} from the two stations (303 K) and fixed ΔH_{eq} (100 kJ mol^{-1}) and ΔH_a (40 kJ mol^{-1}) as described in Appendix A. The soil flux is estimated following Ogée et al. (2016) as implemented by Kooijmans et al. (2021).

13

To examine the humidity impact in SiB4, we performed a simulation with and without the lower threshold for F_{LH} of 0.7 for ENF (see Sect. 2.1.2). Additionally, we replaced the RH at leaf level calculated by SiB4 by RH measured above the canopy.

340   Results will be shown in Sect. 3.5.1. we simulated the global COS leaf uptake without the 0.7 threshold of F_{LH} for ENF.

2.5 Error reduction and statistics

To determine the uncertainty in the optimized model parameters, we employed a Monte Carlo optimization procedure as described in detail in Appendix B. In short, 100 optimizations were performed. In each optimization, we perturbed the state

345   with random Gaussian noise on the state and the observations (Chevallier et al., 2007; Bosman and Krol, 2022), according to the errors in the state and observations (Fig. 4). Posterior error statistics will be reported in Table 3.

Additionally, we quantified the performance of the optimization by calculating the root mean square errors (RMSEs), mean bias errors (MBEs), and the chi-square metric (χ^2). The χ^2 metric quantifies the average deviation from the observations,

350   expressed in σ_y units. Thus, $\chi^2=1$ signal that, on average, the model fits the observation within 1σ indicating a realistic error setting.

3. Results and discussion

3.1 Impact of each conductance

355   Figure 5 investigates which conductance contributes most to the total conductance (g_t). In these plots, all conductances are prior values before optimization. g_s and g_{CA} were derived from observations (Sect. 2.2.2). We find that g_t is determined mainly by g_{CA} and g_s. During daytime, g_{CA} is the lowest conductance in almost all months in Hyytiälä but is comparable to g_s in Harvard Forest. The value of g_b is the highest and hence has the smallest impact on g_t. This finding supports this study's proposed two-step optimization process to improve g_s and g_{CA} (see Sect. 2.3).
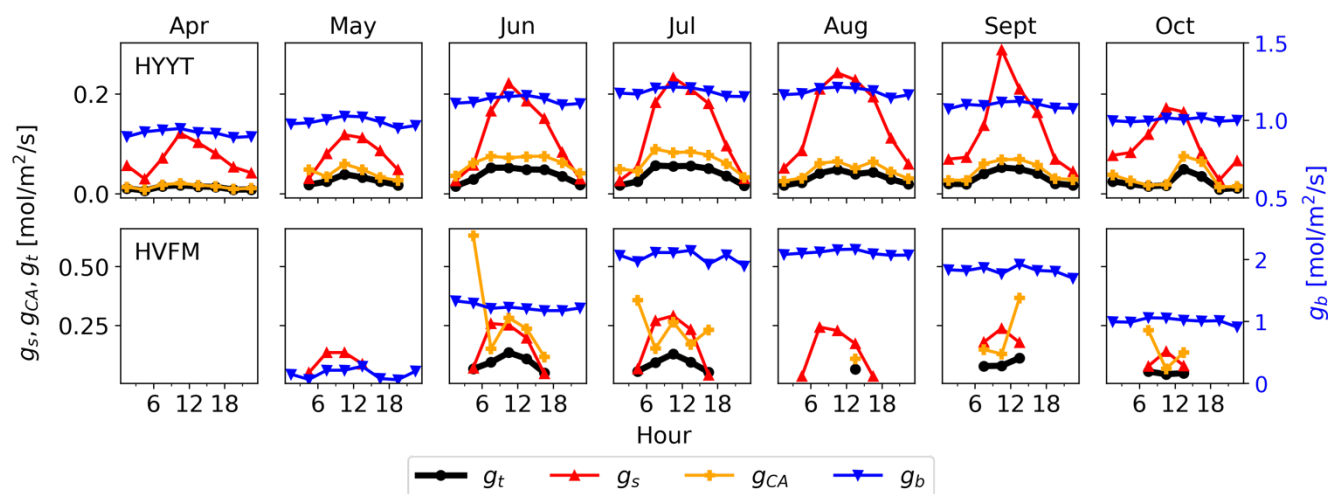
360

Figure 5. Monthly averaged diurnal variation of conductances (black: g_t, red: g_s orange: g_{CA}, blue: g_b) in Hyytiälä (HYYT) and Harvard Forest (HVFM). g_b is estimated by SiB4, g_s and g_{CA} are calculated based on observations as described in Sect. 2.2.2. Negative values are not displayed. The total conductance g_t is calculated from g_b, g_s, and g_{CA} according to Eq. (1).

365 **3.2 Optimization performance**

We obtained optimized parameters after five iterations. By design, the optimized results reduced the deviations between model and observation of GPP and COS leaf uptake. This improvement is quantified by statistical indexes in Tables 1 and 2, respectively. GPP_{BB} is improved compared to the prior (Table 1), with a slight RMSE reduction from 5.51 to 4.87 $\mu mol\ m^{-2}\ s^{-1}$ and a MBE reduction from 0.69 to 0.04 $\mu mol\ m^{-2}\ s^{-1}$ (Table 1). The χ^2 was reduced from 0.88 to 0.80. The

370 improvement in GPP_{BB} reflects the effect of optimizing b_1 and b_0 in the BB model.

Table 1. RMSE, MBE, and χ^2 for the estimation of GPP_{BB} in daytime using prior stomata parameters (Pri) and posterior parameters (Post).

| Type	RMSE ($\mu mol\ m^{-2}\ s^{-1}$)	MBE ($\mu mol\ m^{-2}\ s^{-1}$)	χ^2
Prior (Pri)	5.51	0.69	0.88
Posterior (Post)	**4.87**	**0.04**	**0.80**

375 The posterior result of COS leaf uptake ("Post" in Table 2) shows a slight improvement compared to the original state variables with $f(T_{can})_{new}$ in RMSE (from 8.23 to 6.43 $pmol\ m^{-2}\ s^{-1}$) but significantly improved MBE (from -4.65 to -0.34 $pmol\ m^{-2}\ s^{-1}$, see "Post" in Table 2). The large RMSE reflects the typically large random noise of COS flux observations (Kooijmans et al., 2016; Kohonen et al., 2020). However, χ^2 drops from 1.01 to 0.61, confirming that the optimization properly reduced the mismatch between observations and the model within the error statistics. Figure 6 compares the optimized COS

380 leaf uptake to the original SiB4 simulation in scatter plots. Where the original simulation with $f(T_{can})_{SiB4}$ and previous state

15

variables was often underestimating the observations, the optimized results resemble the observations over a larger range of the data.

Table 2. Same as Table 1 but for COS leaf uptake, as applied in the original f(T_{can})$_{SiB4}$ simulation with original conductance parameters (Org), with the new temperature response function $f(T_{can})_{new}$ using the initial g_s and g_{CA} parameters (Pri), with optimized parameters (Post). Here, state parameters relevant for g_{CA} are α and T_{eq}. The state parameters relevant for g_s are b_0 and b_1.

Type	g_{CA} f(T)	RMSE ($pmol\ m^{-2}\ s^{-1}$)	MBE ($pmol\ m^{-2}\ s^{-1}$)	χ^2
Previous SiB4 (Org)	$f(T)_{SiB4}$	8.23	-4.65	1.01
Prior (Pri)	$f(T)_{New}$	6.71	1.32	0.66
Posterior (Post)		6.43	-0.34	0.61
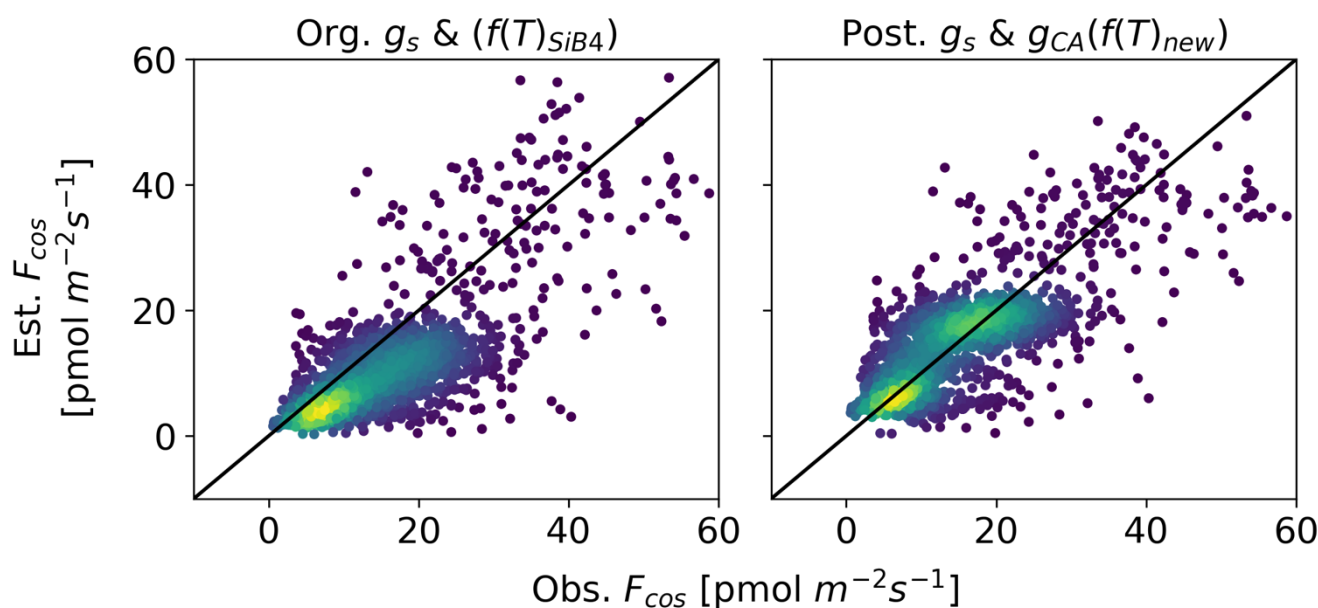
Figure 6. Scatter plots between observed and estimated COS leaf uptake from original parameters with $f(T_{can})_{SiB4}$ (left) and optimized parameters with $f(T_{can})_{new}$ (right). The colors represent the density of data.

3.3 Optimized parameters

The optimized parameter values with posterior errors are listed in Table 3. The optimized SiB4 parameters differ between the stations, likely because the dominant PFT and the climate conditions differ between Hyytiälä and Harvard Forest. For instance, the optimized T_{eq} is smaller in Hyytiälä (295 K) than in Harvard Forest (311 K). Thus, the optimum temperature reflects the temperature dependence of the enzyme and its adaptation to temperature (Lee et al., 2007). This indicates that regional climate information is important for the correct estimation of g_{CA}. The range of T_{eq} can be compared with other COS soil models. For

instance, Ogée et al. (2016) used the same prescribed value for ΔH_a and they adopt T_{eq} as 298 K, which is in the middle of our
400   optimized temperatures for Hyytiälä and Harvard Forest.

The α, which is the enzyme activity of CA relative to the V_{max} of RuBisCo, is reduced from 1400 to 1316 (in growth) and 1331
(in maturity) in Hyytiälä. In Harvard Forest, α values are larger than the original values in SiB4 for leaf-out (1798), growth
(1740), and maturity (2224) phenological stages. Here it should be noted that the change of α should be interpreted in
405   combination with the new temperature function $f(T_{can})_{new}$ of g_{CA}. Since we only optimize T_{eq} for two PFTs (with identical and
fixed values for ΔH_a and ΔH_{eq}) and T_{eq} only shifts $f(T_{can})_{new}$ (Fig. 1), the magnitude of g_{CA} is primarily determined by parameter
α. Since the observed COS leaf uptake in Harvard Forest is larger than in Hyytiälä, larger values of α are derived for Harvard
Forest. The different values of α derived for different phenological stages will be discussed in Sect. 3.4.

410   The optimized results of the BB model parameters b_0 are similar but b_1 values are mostly higher than the original values used
in SiB4. The parameter b_0 for Hyytiälä (0.013 mol m^{-2} s^{-1}) and Harvard Forest (0.007 mol m^{-2} s^{-1}) are higher and smaller
compared to the initial value (0.010 mol m^{-2} s^{-1}). For the optimized BB model parameter b_1, the empirical slope between g_s
and GPP, we find a considerable increase in Hyytiälä (16.38) and a slight increase in Harvard Forest (11.43), compared to the
prescribed SIB4 value of 9.0. Our optimized values are larger than the values presented in a review paper for the evergreen
415   gymnosperm tree which showed $b_1 = 6.8$ and are similar to $b_1 = 8.7$ for the deciduous angiosperm tree (Miner et al., 2017).
As will be discussed in Sect. 3.5, the higher slope in Hyytiälä is possibly related to an incomplete separation of observed
transpiration rates from the latent heat flux.

Concerning the estimated errors in b_0, b_1, and T_{eq}, we find that errors have been reduced significantly compared to the prior
420   error range. This indicates that the available data constrain these parameters well. Only the α parameters of Harvard forest are
less well constrained. Also, the skill of the optimization to independently optimize the parameters is high, as quantified by the
posterior covariances that are presented in Appendix B.

Table 3. Original (Org) and optimized (Post) state vectors for Hyytiälä and Harvard Forest in different phenological stages as defined
425   **by SiB4. Values of Posterior in parenthesis indicates posteriori errors. Detailed error reduction is described in Appendix B.**

Approach	State vector	Hyytiälä		Harvard Forest		
		Growth	Maturity	Leaf-out	Growth	Maturity
Previous SiB4 (Org)	V_{max} of RuBisCo (μmol m^{-2} s^{-1})	52	54	96	94	92
	α (-)			1400		
	b_0 (mol m^{-2} s^{-1})			0.01		
	b_1 (-)			9.0		
Prior	α (-)	1400 ($\pm$ 1000)		2000 ($\pm$ 1000)		

(Pri)	b_0 (mol m⁻² s⁻¹)	0.02 (± 0.02)		0.01 (± 0.02)		
	b_1 (-)	17 (± 5)		12 (± 4)		
	T_{eq} (K)	295 (± 20)		310 (± 20)		
Posterior (Post)	α (-)	1316 (± 509)	1331 (± 574)	1798 (± 527)	1740 (± 494)	2224 (± 613)
	b_0 (mol m⁻² s⁻¹)	0.013 (± 0.009)		0.007 (± 0.006)		
	b_1 (-)	16.36 (± 2.87)		11.43 (± 1.98)		
	T_{eq} (K)	295 (± 11)		311 (± 10)		

3.4 Optimized temperature response

The optimized parameters show significant improvement in temperature response of the COS leaf uptake. Figure 7 presents the temperature dependency of g_{CA} and COS leaf uptake from the original and optimized simulations output and observations.

430 The observed COS leaf uptake and pseudo-observations g_{CA} (details in Sect. 2.2.2) in Hyytiälä show a decrease above 20 ℃. As stated before, the original $f(T_{can})_{SiB4}$ describes the CA enzyme activity as an exponentially increasing response to temperature, which does not resemble the observations. The optimized g_{CA} and COS leaf uptake follow the temperature dependence of the observation more closely than the original $f(T_{can})_{SiB4}$. In Harvard Forest, an underestimated bias is shown at a lower temperature under 10 ℃, mostly corresponding to nighttime. This underestimate is related to the uncertainty in

435 nighttime g_S and the small data volume at low temperatures (details in Sect. 2.2.2).

In the upper panel of Fig. 7, we see the different roles of α and $f(T_{can})_{new}$ in the improvement of g_{CA} response to temperature as the red and orange lines. Without the α correction applied (Posterior with α = *1400*; orange line), the optimized g_{CA} resembles the fluctuations in the observations but there remains a bias in the amplitude. In contrast, when the optimized value of α is

440 included, the amplitude of g_{CA} is improved (red line). Due to the different optimized α values in each phenological stage, the improvement of the red line shows the appropriate temperature responses. For instance, in Harvard Forest, α in leaf-out and growth (1798 and 1740) mostly corresponds to lower temperatures. At these stages, the impact on g_{CA} is smaller because g_{CA} is smaller than that at high temperature. At high temperatures there are more significant corrections of g_{CA}, which correspond to the maturity stage value of α (2224).

445

The temperature responses of g_{CA} and COS leaf uptake now show an optimum temperature in Hyytiälä, characterized by the parameter T_{eq} (*T = 295 K (22 ℃)*). In addition, the improvement is significant at temperatures both below and above the optimum temperature in Hyytiälä. The optimized g_{CA} is larger throughout the whole temperature range in Harvard Forest,

without an optimum within the measured range. This corresponds to $T_{eq} = 311\ K\ (38\ ^oC)$, a value substantially higher than

450   found at Hyytiälä.

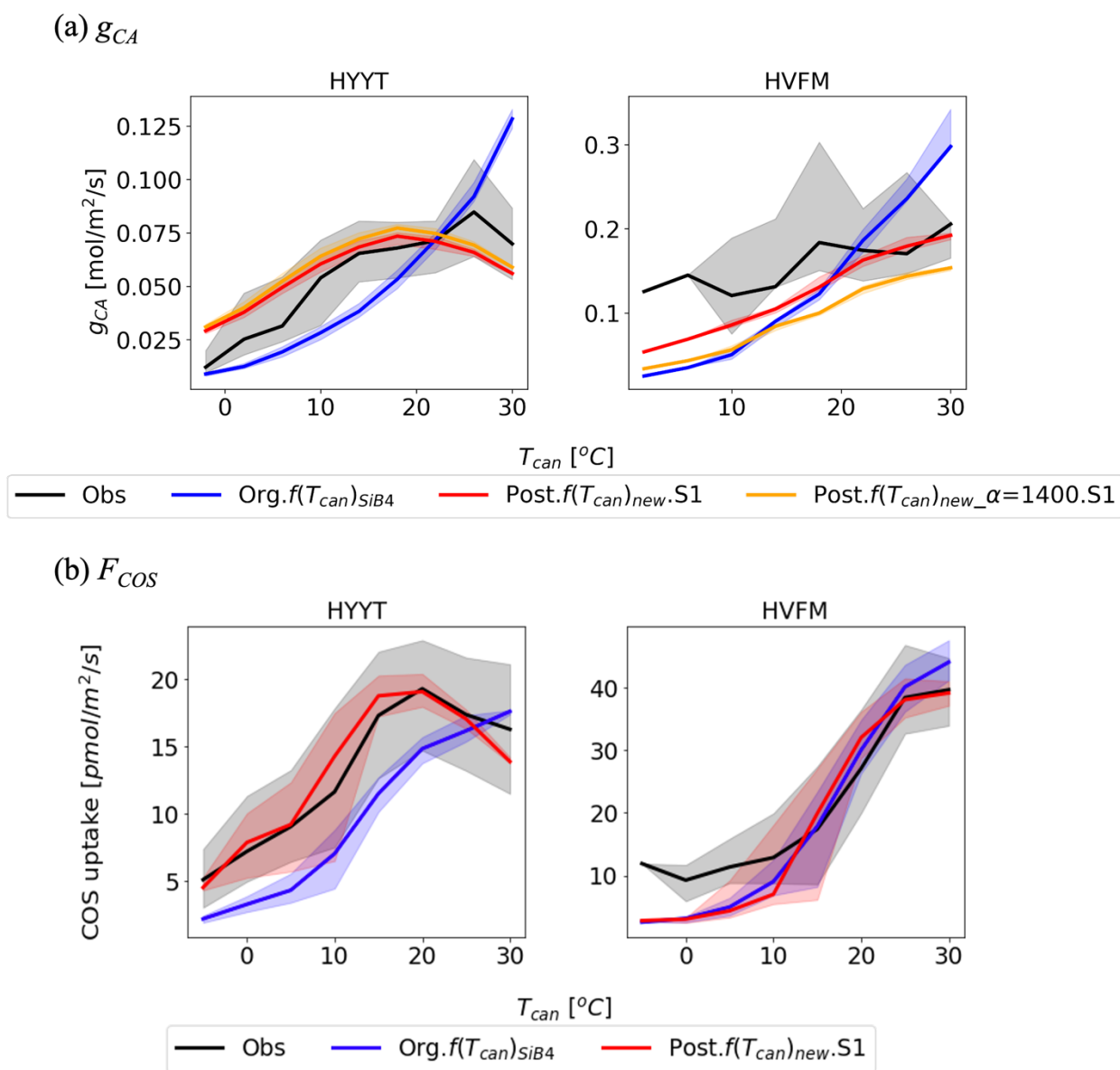(a) g_{CA}

(b) F_{COS}

Figure 7. Temperature dependency on g_{CA} (a) and COS leaf uptake (b) in Hyytiälä (HYYT, left) and Harvard Forest (HVFM, right). The lines are medians and the filled area represents the 25 to 75 percentiles of each temperature range with 3 ºC intervals. Black: data based on observations; blue: previous parameters with $f(T_{can})_{SiB4}$; red: optimized parameters with $f(T_{can})_{new}$ and g_s parameters of the BB model; orange: same as the red line but now α is prescribed with original value (1400) and not optimized.

19

3.5 Application in SiB4

455   ### 3.5.1 Stationary monthly diurnal variation

Figures 8 and 9 display the SiB4 simulation results obtained with the original and optimized parameterizations compared to observations for Hyytiälä and Harvard Forest, respectively. As a result of the optimization, the monthly diurnal variation of the optimized COS vegetation flux, g_s, and g_{CA} are closer to observations than the original SiB4 simulations. The observed COS leaf uptake and g_s show diurnal and seasonal fluctuations at both measurement sites, with the highest values around
460   midday and in summer. For g_{CA}, we observe a weak diurnal cycle throughout the year, and higher daytime maximum values in summer, driven by the temperature dependence of CA.

In Hyytiälä, COS leaf uptake in the original SiB4 model was underestimated during daytime in all months. The fluxes increased too slowly in the morning for all months (Fig. 8(a)). These issues are solved by optimizing the BB model parameters and
465   temperature response function. In the case of g_s (Fig. 8(b)), the original SiB4 simulation showed the correct timing of the increase and decrease of g_s in the morning and afternoon, but underestimated the peak daytime values. The optimized model now better resembles the daytime g_s values.

However, the model still overestimates g_s in the late afternoon of summer months at Hyytiälä. We speculate that one of the
470   reasons lies in an inaccurate humidity, or humidity stress in SiB4. Figure 10 shows a diurnal cycle of g_s simulations averaged from April to August with different choices on how the humidity stress factor is treated (Sect. 2.5). When the default 0.7 threshold of humidity stress (F_{LH}) in ENF is applied in SiB4, g_s is overestimated in the afternoon in Hyytiälä (blue dotted line). When we removed the minimum threshold of F_{LH} for ENF, g_s simulations during mid-day are improved (note that the threshold was only implemented for ENF, not for DBF, and thus the blue dotted line is not visible for Harvard Forest in Figure 10).
475   However, SiB4 still tends to overestimate g_s in the morning and late afternoon. In contrast, when we base the g_s calculation on the observed RH above the canopy, the diurnal cycle is better simulated (orange dashed line). This implies that SiB4 has the tendency to underestimate the humidity stress in the late afternoon when converting observed specific humidity above the canopy to humidity at leaf surface level.

480   The optimized model still significantly underestimates g_s at Hyytiälä in April, September, and October (Fig. 8b). This might indicate that we did not properly separate stomatal transpiration rates from the observed latent heat flux. The simulated mean ratios of evaporation to evapotranspiration in these three months are 66 %, 60 %, and 95 %, respectively, and these values are higher compared to the other months (43 to 53 %). Thus, we speculate that the observed evapotranspiration does not solely represent stomatal transpiration in these months, leading to overestimated g_s in the observation.

485

Figure 8(c) shows that the optimized g_{CA} often resembles the observed daytime g_{CA} better than the original SiB4 simulation. Only in April is the optimized g_{CA} overestimated in Hyytiälä. Again, this can likely be explained by the underestimated g_s, which is used to derive pseudo-observations of g_{CA} (see Sect. 2.2.2).
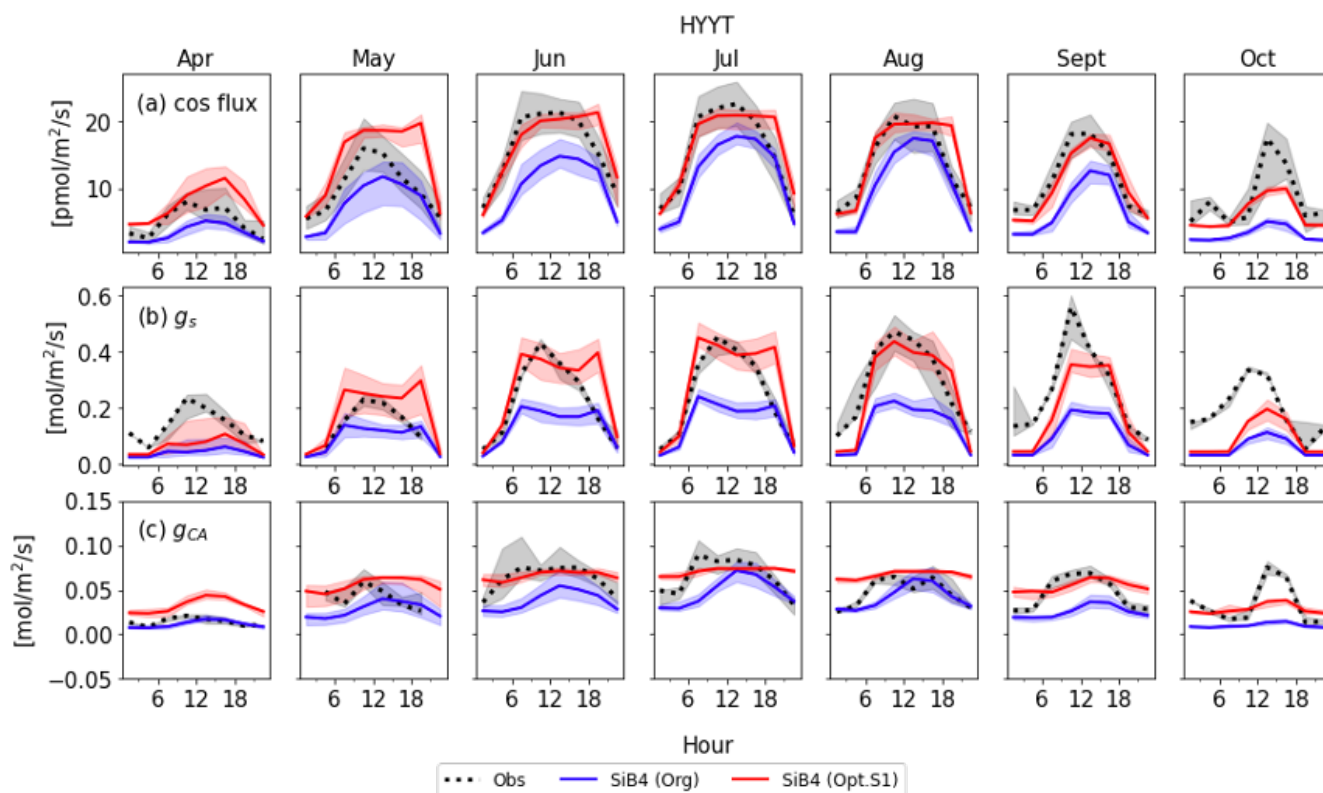

Figure 8. Monthly-diurnal cycle of COS leaf uptake (a), g_s (b), and g_{CA} (c) in Hyytiälä (HYYT) from 2012 to 2016. Data include observations (black dots), the original SiB4 model with $f(T_{can})_{SiB4}$ (blue solid), and SiB4 with optimized g_s and g_{CA} parameters with $f(T_{can})_{new}$ (red solid). The filled area corresponds to the 25-75 percentile of the data in each three-hourly interval of each month.

490

At the Harvard Forest, the optimized SiB4 model generally simulates the magnitude of the COS leaf uptake well (Fig. 9(a)). The model overestimates the COS leaf flux only in the afternoon during the summer months. However, g_s values are generally overestimated and SiB4 simulates two peaks during daytime, indicating humidity stress only shortly at mid-day. However, in reality, the humidity stress likely remains a limiting factor in the afternoon under conditions with high vapor pressure deficit

495 (VPD). Observations show that g_s typically peaks in the early morning and decreases in the afternoon due to higher afternoon VPD. Figure 10 shows that, similar to the Hyytiälä simulation, the afternoon decrease in g_s at Harvard Forest is better simulated when we use the RH observed above the canopy. In Fig. 9(c), the optimized g_{CA} during the daytime agrees well with the pseudo-observations, except for several drops or peaks in July and October, likely caused by observational errors or uncertainty of the observed g_s.
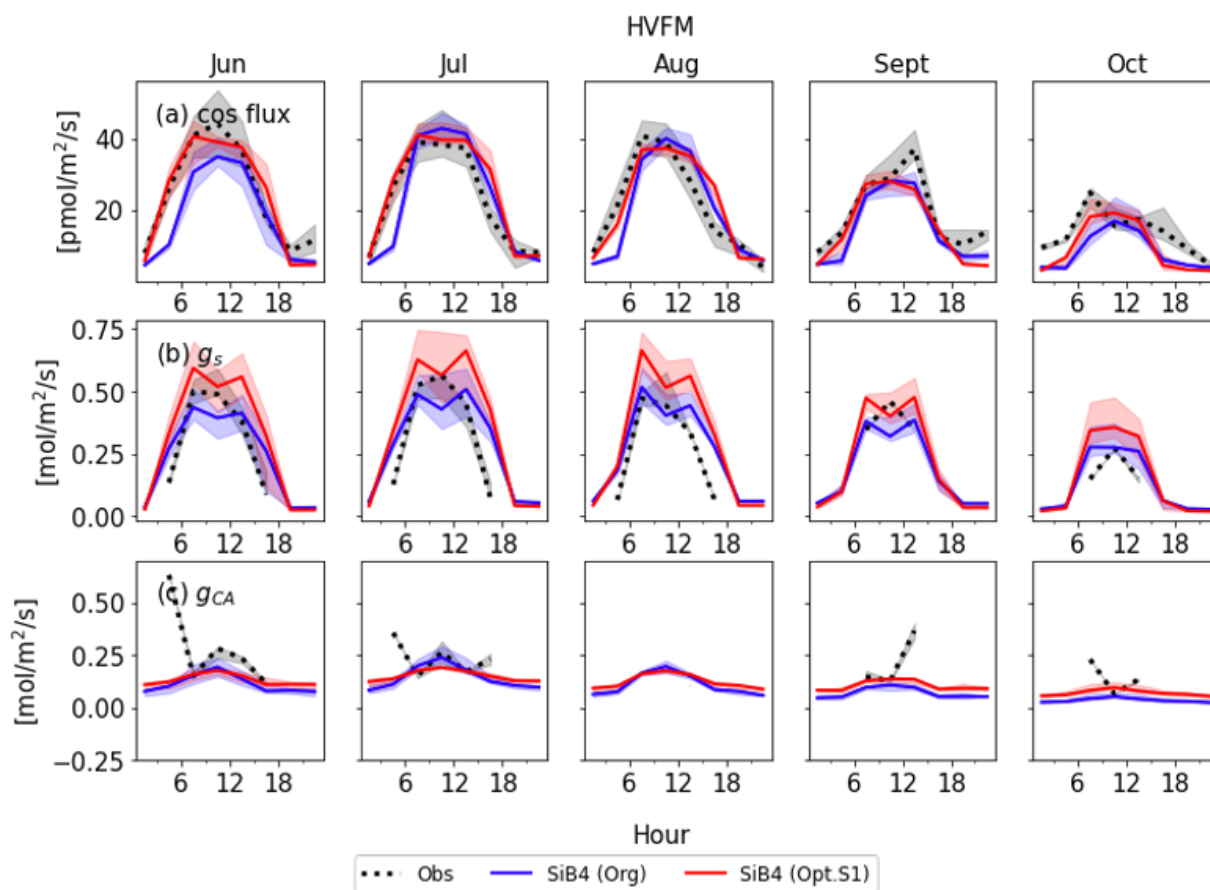
21

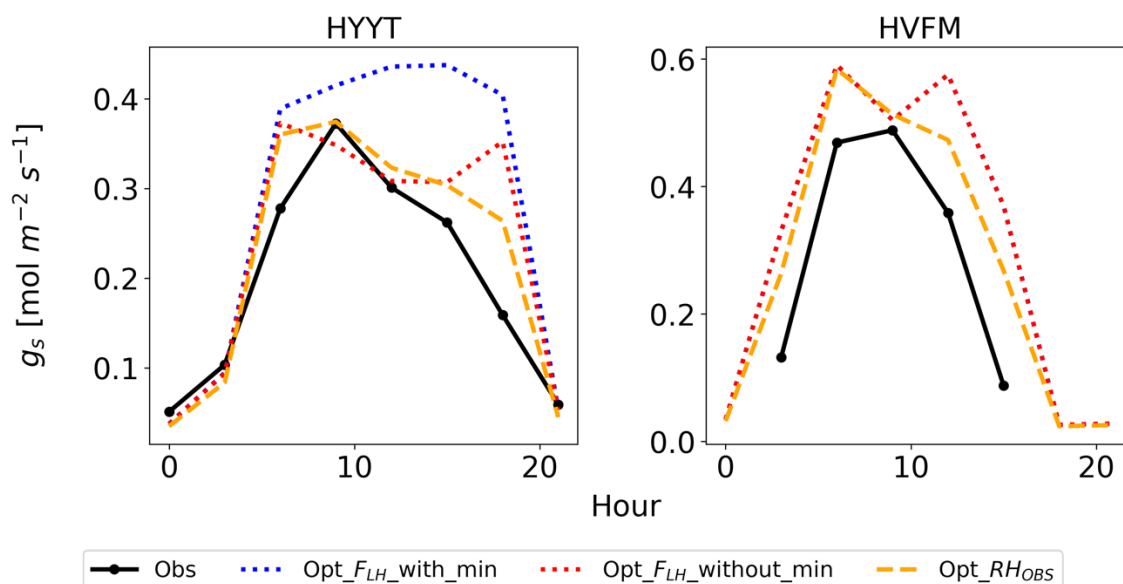**Figure 9. Same as Fig. 8 but for Harvard Forest (HVFM).**

Figure 10. Average diurnal cycle of g_s in Hyytiälä (HYYT) and Harvard Forest (HVFM) from April to August. Data include observations (black solid), SiB4 simulation with optimized parameters with minimum bounds of F_{LH} (blue dotted), without bounds (red dotted), and with observed RH in air (orange dashed). Note that the blue and red lines overlap for HVFM.

3.5.2 Global application

Figure 11 shows the biosphere COS flux (soil and the optimized vegetation flux) using the optimized parameters and the difference with the original SiB4 model. In general, the COS biosphere uptake is lower in the tropics and higher towards high latitudes in the SiB4 model with optimized parameters. We find the same patterns for all seasons. The differences are consistent with canopy temperature variations. When temperatures are below 3 °C (boreal) and 3-25 °C (temperate), the optimized COS biosphere uptake is larger compared to the original simulation, corresponding with higher g_{CA} values calculated by the new temperature function in Fig. 7. In contrast, temperatures above about 25 °C result in lower COS biosphere uptake in the optimized run, reflecting the reduced enzyme activity at high temperatures in the new temperature response function. Note here that we also found that the temperature response of CA is different in different climate zones. Since we do not have observations in the tropics, the calculated lower uptake in the tropics remains very uncertain. The higher uptake at high latitudes and lower uptake at the tropics are nevertheless consistent with inverse modelling results presented in Ma et al. (2021) and would help towards closing the COS budget. Still, however, the temperature response function and BB parameters are now based on measurements of only two sites in only two biomes. With more measurements over different vegetation types, these parameters could also be optimized for a wider range of ecosystems.

23
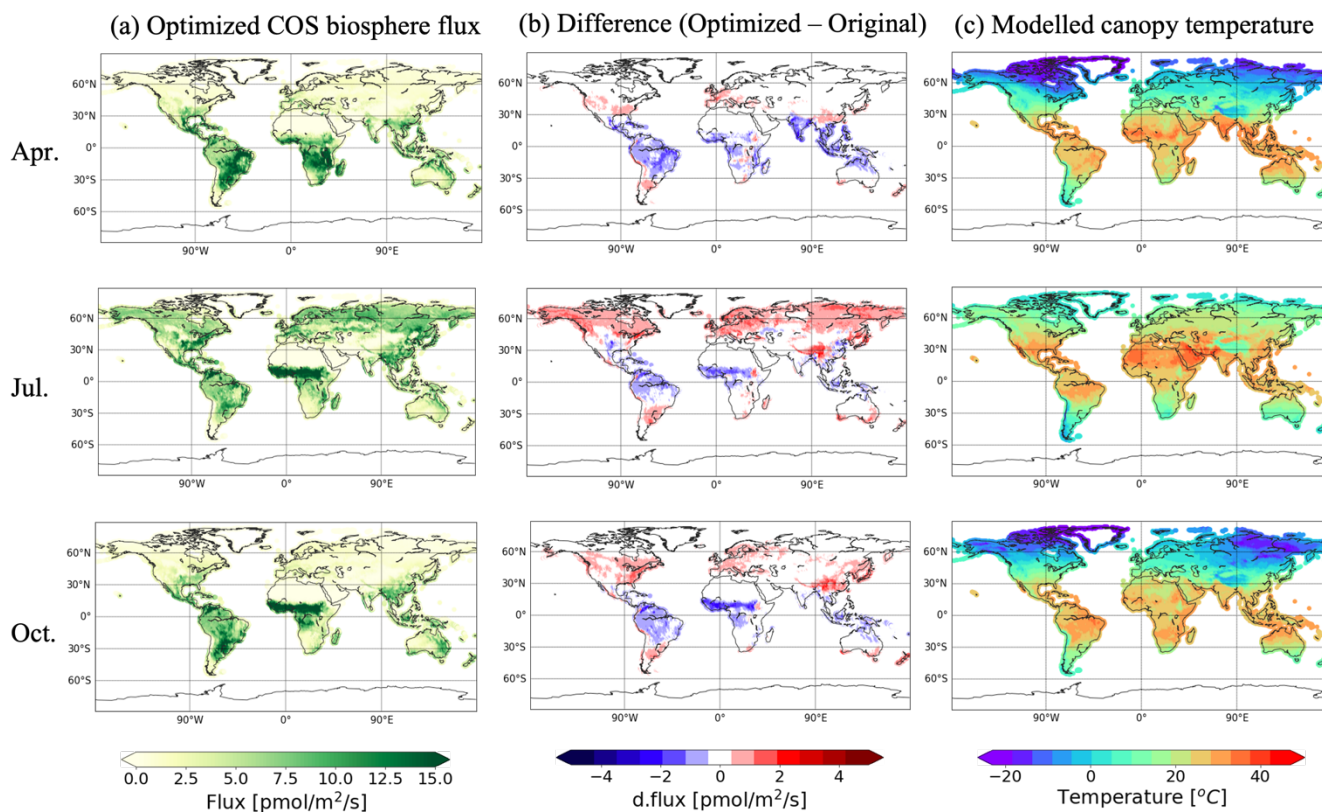
Figure 11. Spatial distribution of optimized COS biosphere fluxes (a), the difference between optimized and original COS biosphere flux (b), and canopy temperature (c). All were estimated by the SiB4 model.

4. Conclusion

To simulate more accurate COS leaf uptake in the SiB4 model, we have proposed a new temperature function $f(T_{can})_{new}$ for the CA enzyme and have optimized g_s and g_{CA} parameters using observations in ENF (Hyytiälä) and DBF (Harvard Forest) systems. The optimized model reduced the MBE from -4.65 to -0.34 $pmol\ m^{-2}\ s^{-1}$ and reduced χ^2 from 1.01 to 0.61.

The new temperature function is characterized by an optimum temperature of 295 K (22 °C) (Hyytiälä) and 311 K (38 °C) (Harvard Forest) with $\varDelta H_a$ = 40 kJ mol^{-1}. The new function now considers an optimum temperature for enzyme activity, contrary to the initial temperature function used in SiB4 where an exponential increase of the temperature function was adopted from the RuBisCo enzyme activity. The new temperature response increases g_{CA}, and thereby the COS flux when the temperature is below the optimum temperature (mostly at high latitudes) and decreases the COS uptake at higher temperatures. (e.g. close to the equator). Globally, these modifications help to close gaps in COS budget that were identified in earlier studies.

24

535   In this study, we have interpreted the decreasing g_{CA} at higher temperatures as an optimum enzyme activity with the widely applied assumption that there are no COS emissions in leaves. However, COS emissions have recently been reported at high temperatures (Maseyk et al., 2014, Commane et al., 2016, Gimeno et al., 2017). To determine reasons for reducing COS leaf flux and internal conductance at high temperatures, it will be necessary to analyze the possibility that leaf emissions exist in observations in the future.

540

We have optimized the BB model parameters for which we took advantage of the characteristics that the nighttime COS flux informs about nighttime g_s, and thus the parameter b_0. The improved correspondence between model and observations shows that COS observations can help to constrain the relation between g_s and GPP better. In addition, we showed that SiB4 underestimates the leaf humidity stress under conditions where high VPD should limit g$_s$ in the afternoon. This can be improved

545   with more accurate relative humidity values and removing the threshold of humidity stress that was implemented in SiB4 specifically for ENF.

The optimized parameters show different values depending on the PFT. Therefore, extending our approach with more observations in different climate zones and over different PFTs will help obtain accurate COS fluxes on a global scale. This

550   approach would reduce the uncertainty in the global COS budget and provide additional constraints on GPP.

### Appendix A. State variable error settings

To evaluate the impact of the various parameters in $f(T_{can})_{new}$ in the optimization as state variables, we implemented a sensitivity test of a total cost function combined with $cost_1$ and $cost_2$, excluding the background term in the cost function equation (Eq. (10)). Fig. A1 shows the shape of the cost function when one parameter is varied within an acceptable range, while the other

555   parameters are fixed (Daniel et al., 2010; Sun et al., 2015) (details in Sect. 2.3.2). Based on the shape of the cost function, we used a pragmatic approach to select realistic parameter ranges. Variable values that push the cost function beyond 3.45 (Hyytiälä) and 5.14 (Harvard Forest) were considered outside the allowed physical range (red lines in Fig. A2). These thresholds are determined by the cost function value assuming that the modelled $H(x)$ is the 75-percentile value of observation in three-hourly observation in each month. Variables α, b_0, b_1, and T_{eq} (Fig. A1(a), (b), (c), and (f)) have more significant

560   impacts on the cost function than ΔH_a (Fig. A1(d)) and ΔH_{eq} (Fig. A1(e)). Overall, costs in Harvard Forest are higher than in Hyytiälä, likely because DBF has larger diurnal and seasonal variations in the observed fluxes than ENF. We set the optimization range as an initial value $\pm$ 1.5 state error to apply SHGO algorithm.

Figure A2 shows contour diagrams of the cost function as a function of T_{eq} and other parameters of $f(T_{can})_{new}$. The gradient is

565   the cost function indicates the relative importance of each parameter. ΔH_{eq} does not interact with T_{eq}, but ΔH_a is inverse

proportional to T_{eq} to minimize the cost. The cost function is most sensitive to variations in T_{eq} and therefore we decided to fix ΔH_{eq} and ΔH_a at 100 kJ mol^{-1} and 40 kJ mol^{-1}, respectively and to base our optimization on the state variables α, b_0, b_1 and T_{eq}.
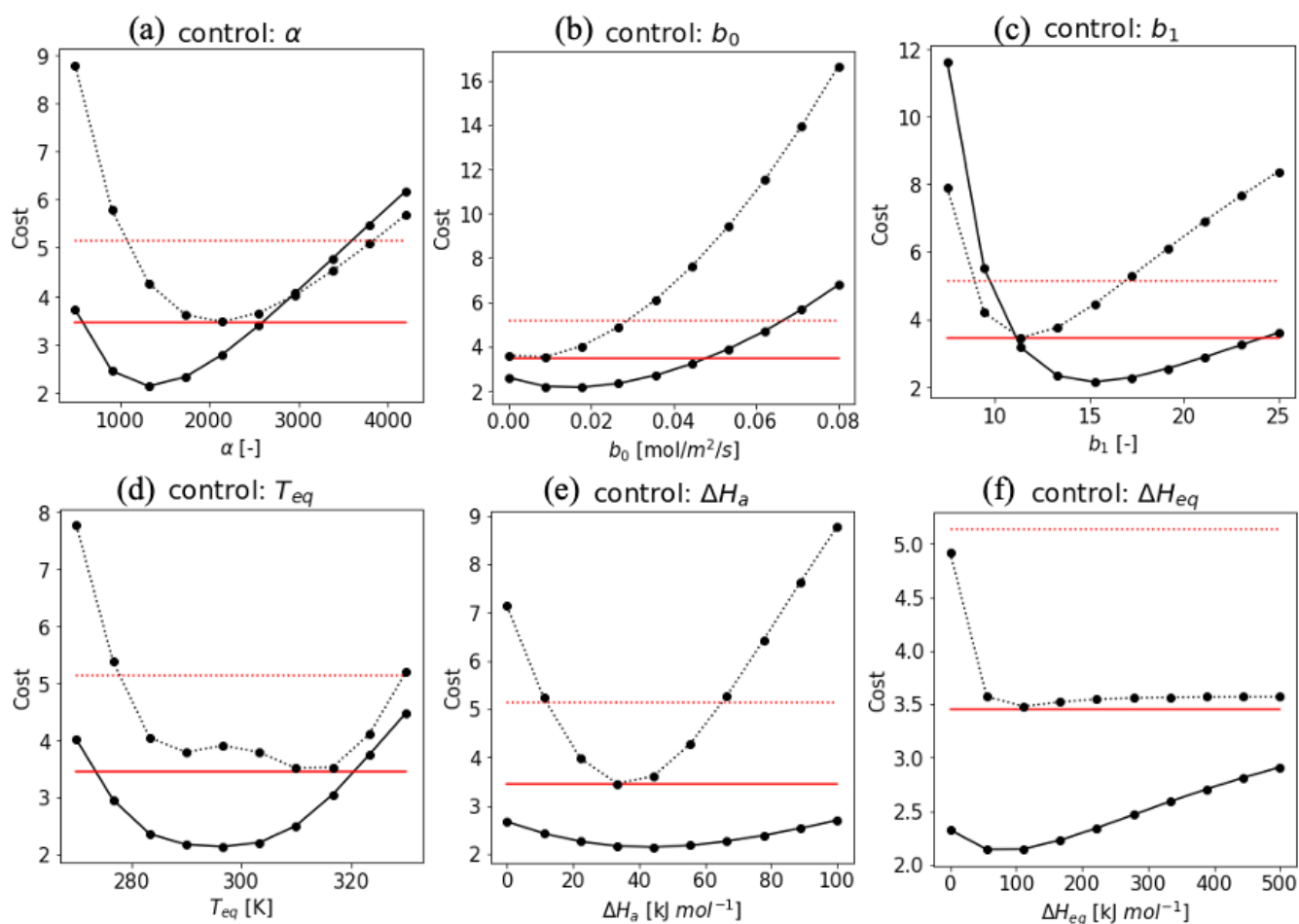
Figure A1: Cost function values plotted against the value of the state vectors elements in Hyytiälä (solid line) and Harvard Forest (dotted line). The red lines indicate a criteria cost calculated by $H(x)$ as the 75-percentile value of every three-hourly observation in each month. While the target parameter changes, the other variables are fixed as α = 1400 (Hyytiälä), 2000 (Harvard Forest), ΔH_a = 40 kJ mol^{-1} ΔH_{eq} = 100 kJ mol^{-1}, and T_{eq} = 295 K (Hyytiälä), 310 K (Harvard Forest), b_0 = 0.02 (Hyytiälä), 0.01 (Harvard Forest), and b_1 = 17 (Hyytiälä), 12 (Harvard Forest). These values were decided where the cost has minimum.

(a) T_{eq} v.s. ΔH_{eq}

(b) T_{eq} v.s. ΔH_a
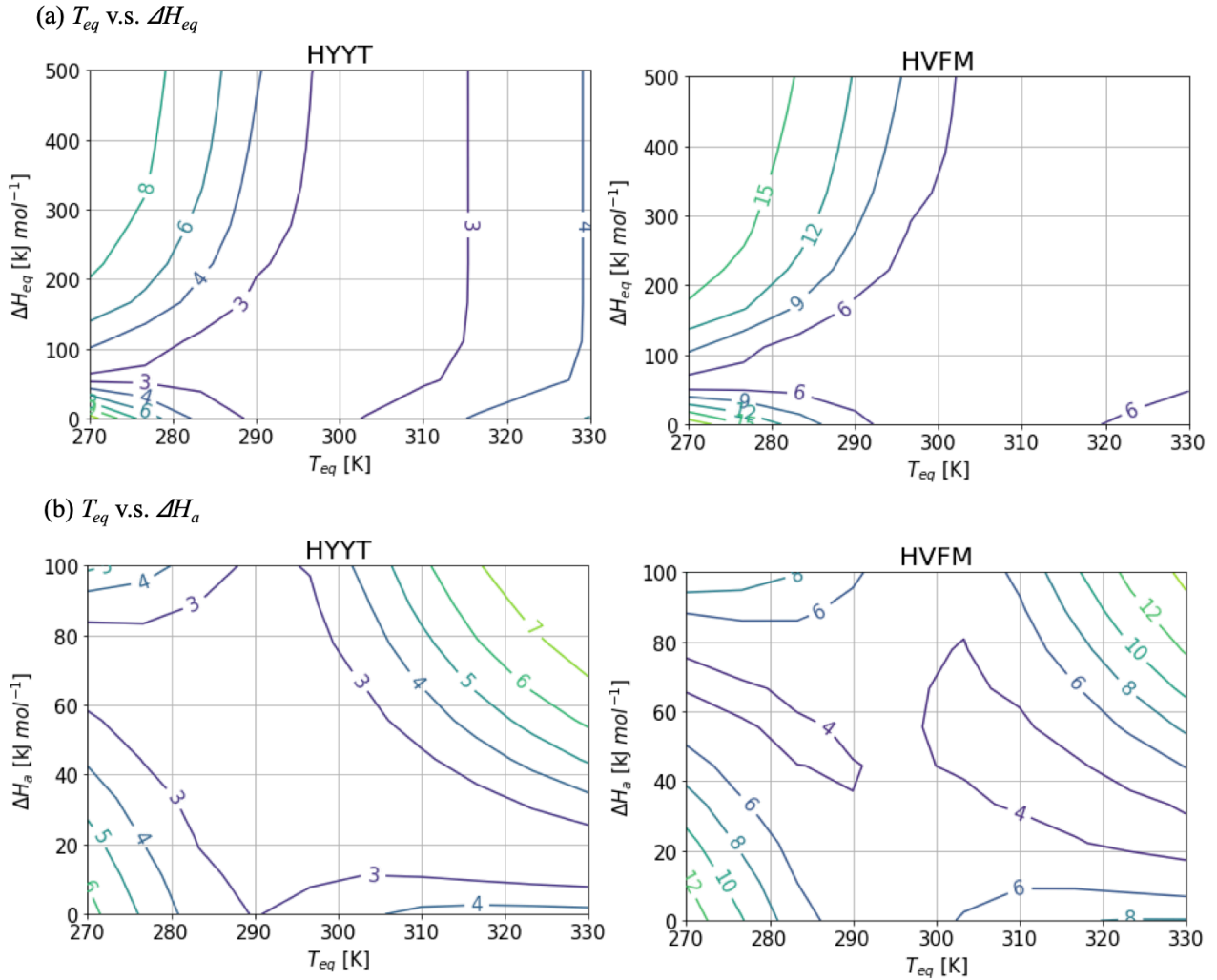
Figure A2: Contour diagram of the cost function value as a function of T_{eq} and (a) ΔH_{eq} and (b) ΔH_a in Hyytiälä (left) and Harvard Forest (right). While the target parameter changes, the other variables are fixed as Figure A1.

Appendix B. Posterior uncertainties

580   To evaluate the ability of constrain the parameters, we performed an ensemble optimization with 40 different members. In each optimization, noise was added to the parameters (ε_a) and to the observation (ε_y). Random perturbations were drawn from a normal distribution with zero mean and standard deviations σ_a for the state parameters and σ_y for the observations. The new cost function of an individual optimization thus becomes:

$$J(x) = \frac{(x - x_a + \varepsilon_a)^2}{2\sigma_a^2} + \frac{\left(y + \varepsilon_y - H(x)\right)^2}{2\sigma_y^2} \tag{12}$$

585 We optimized each ensemble with the same observations (GPP and COS leaf uptake) and state variables but added noise to
each ensemble member (Chevallier et al., 2007). Subsequently, we calculated the posterior uncertainty as the one-standard
deviation of the posterior distribution of the optimized parameters.

Figure B1 shows the prior and posterior distribution of the parameters at the two stations. All posterior parameters show
590 considerable reductions of variations (error), with optimized values that are listed in the main text, Table 3.

Additionally, we calculated a correlation matrix between the posterior state parameters at the two stations, which is shown in
Fig. B2. Overall, each parameter does not interact significantly (covariances < 0.7) except for parameters b_0 and b_1. b_0 and b_1
influence the g_s calculation in opposite ways. For example, a larger optimized value of b_0 corresponds to a smaller slope b_1.
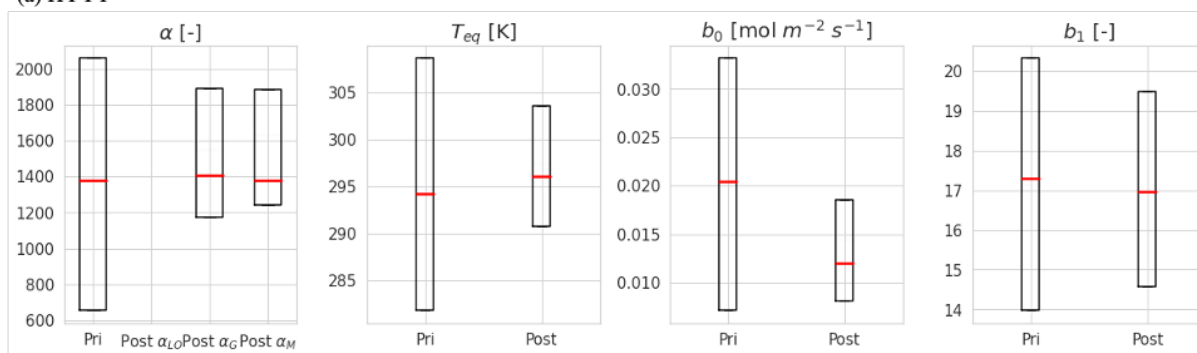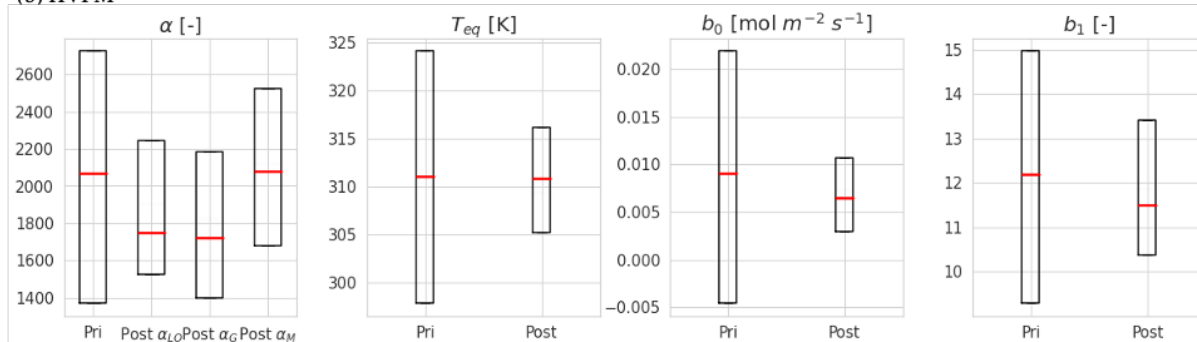
595

**Figure B1. Error reduction of state variables in two stations (Hyytiälä (HYYT) and Harvard Forest (HVFM)). The red lines
represent median values, and the boxes represent errors. Column 'Pri' shows the initial value and state error. Column 'Post'
represents the mean of the optimized state variables and the corresponding standard deviation. α_{LO}, α_G, α_M indicate α in each
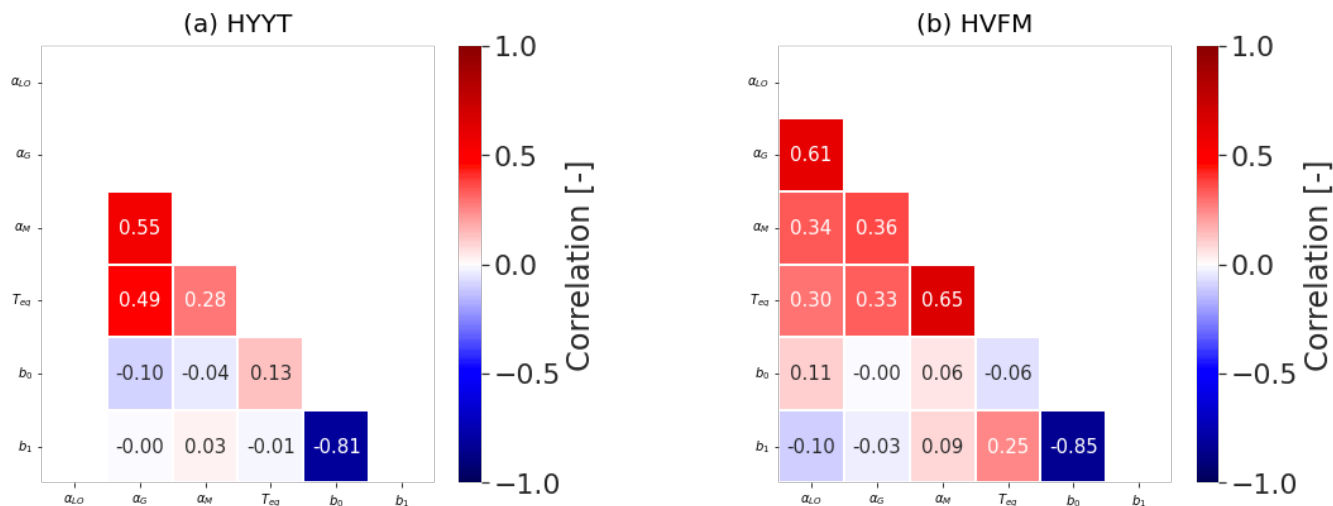phenological stage (leaf-out, growth, and maturity, respectively).**

600

28

Figure B2. Covariance matrix for all state variables in Hyytiälä (HYYT) and Harvard Forest (HVFM).

605

Code availability

The SiB4 code is available online at https:// gitlab.com/kdhaynes/sib4v2_corral. TM5-4DVar model codes are available on the TM5-4DVAR website (https: //sourceforge.net/projects/tm5/).

Author contributions

610 AC, LMJK, and MK devised the study. AC optimized ecosystem parameters and analysed the results with consultation of LMJK and MK. KM and RW provided observation data and site-specific insights. AC wrote the manuscript and all authors provided comments.

Competing interests

The authors declare that they have no conflict of interest.

615

Acknowledgements

29

620 (ACCC) Flagship (Vesala et al., 2022). The soil dataset at Hyytiälä was collected from Sun et al. (2018). Data from Harvard Forest is supported by the AmeriFlux Management Project (Wehr et al., 2017; Commane et al., 2015).

References

Abadie, C., Maignan, F., Remaud, M., Ogée, J., Campbell, J. E., Whelan, M. E., Kitz, F., Spielmann, F. M., Wohlfahrt, G., Wehr, R., Sun, W., Raoult, N., Seibt, U., Hauglustaine, D., Lennartz, S. T., Belviso, S., Montagne, D., and Peylin, P.: Global modelling of soil carbonyl sulfide exchange, Biogeosciences, 19, 2427-2463 https://doi.org/10.5194/bg-19-2427-2022, 2022.
630 Baldocchi, D. D., Luxmoore, R. J., and Hatfield, J. L.: Discerning the forest from the trees: an essay on scaling canopy stomatal conductance, Agr. Forest Meteorol., 54, 197–226, https://doi.org/10.1016/0168-1923(91)90006-C, 1991.

Ball J. T.: An analysis of stomatal conductance. Stanford University, 1988.

Ball, J. T., Woodrow, I. E., and Berry, J. A.: A model predicting stomatal conductance and its contribution to the control of photosynthesis under different environmental conditions, In: Biggins, J. (eds) Progress in Photosynthesis Research. Springer,
635 Dordrecht, 221– 224, https://doi.org/10.1007/978-94-017-0519-6_48, 1987.

Bauerle, W. L., Daniels, A. B., and Barnard, D. M.: Carbon and water flux responses to physiology by environment interactions: a sensitivity analysis of variation in climate on photosynthetic and stomatal parameters, Clim. Dynam., 42, 2539–2554, https://doi.org/ 10.1007/s00382-013-1894-6, 2014.

Belviso, S., Schmidt, M., Yver, C., Ramonet, M., Gros, V., and Launois, T.: Strong similarities between night-time deposition
640 velocities of carbonyl sulphide and molecular hydrogen inferred from semi-continuous atmospheric observations in Gif-sur-Yvette, Paris region, Tellus B, 65, 20719, https://doi.org/10.3402/tellusb.v65i0.20719, 2013.

Berkelhammer, M., Asaf, D., Still, C., Montzka, S., Noone, D., Gupta, M., Provencal, R., Chen, H., and Yakir, D.: Constraining surface carbon fluxes using in situ measurements of carbonyl sulfide and carbon dioxide, Global Biogeochem. Cy., 28, 161–179, https://doi.org/10.1002/2013GB004644, 2014.
645 Berry, J., Wolf, A., Campbell, J. E., Baker, I., Blake, N., Blake, D., Denning, A. S., Kawa, S. R., Montzka, S. A., Seibt, U., Stimler, K., Yakir, D., and Zhu, Z.: A coupled model of the global cycles of carbonyl sulfide and CO2: A possible new window on the carbon cycle, J. Geophys. Res. Biogeosciences, 118(2), 842–852, https://doi.org/10.1002/jgrg.20068, 2013.

Billesbach, D. P., Berry, J. A., Seibt, U., Maseyk, K., Torn, M. S., Fischer, M. L., Mohammad Abu-Naser, and Campbell, J. E.: Growing season eddy covariance measurements of carbonyl sulfide and CO_2 fluxes: COS and CO_2 relationships in

650   Southern Great Plains winter wheat, Agr. Forest Meteorol., 184, 48–55, https://doi.org/10.1016/j.agrformet.2013.06.007, 2014.

Burnell, J. N. and Hatch, M. D.: Low bundle sheath carbonic anhydrase is apparently essential for effective C4 pathway operation, Plant Physiol., 86, 1252–1256, https://doi.org/10.1104/pp.86.4.1252, 1988.

Caird, M. A., Richards, J. H., and Donovan, L. A.: Nighttime stomatal conductance and transpiration in C3 and C4 plants, Plant Physiol., 143, 4– 10, https://doi.org/10.1104/pp.106.092940, 2007.

655   Chevallier, F., Bréon, F. M., and Rayner, P. J.: Contribution of the Orbiting Carbon Observatory to the estimation of CO_2 sources and sinks: Theoretical study in a variational data assimilation framework, J. Geophys. Res., 112, D09307, https://doi.org/10.1029/2006JD007375, 2007.

Cochavi, A., Amer, M., Stern, R., Tatarinov, F., Migliavacca, M., and Yakir, D.: Differential responses to two heatwave intensities in a Mediterranean citrus orchard are identified by combining measurements of fluorescence and carbonyl sulfide

660   (COS) and CO_2 uptake, New Phytol., 230, 1394–1406, https://doi.org/10.1111/nph.17247, 2021.

Collatz, G. J., Ribas-Carbo, M., and Berry, J. A.: Coupled photosynthesis-stomatal conductance model for leaves of C4 plants, Funct. Plant Biol., 19(5), 519–538, https://doi.org/10.1071/PP9920519, 1992.

Commane, R., Herndon, S. C., Zahniser, M. S., Lerner, B. M., McManus, J. B., Munger, J. W., Nelson, D. D., and Wofsy, S. C.: Carbonyl sulfide in the planetary boundary layer: Coastal and continental influences, J. Geophys. Res.-Atmos., 118, 8001–

665   8009, https://doi.org/10.1002/jgrd.50581, 2013.

Commane, R., Meredith, L. K., Baker, I. T., Berry, J. A., Munger, J. W., Montzka, S. A., Templer, P. H., Juice, S. M., Zahniser, M. S., and Wofsy, S. C.: Seasonal fluxes of carbonyl sulfide in a midlatitude forest, P. Natl. Acad. Sci. USA, 112(46), 14162– 14167, https://doi.org/10.1073/pnas.1504131112, 2015.

Commane R, Wofsy S, Wehr R.: Fluxes of carbonyl sulfide at Harvard Forest EMS tower since 2010. Harvard Forest Data

670   Archive: HF214 (v.10). Environmental Data Initiative: https://doi.org/10.6073/pasta/b43072ec4b5dbf1f069983e3d5d36a1b, 2016.

Daniel, R. M., Peterson, M. E., Danson, M. J., Price, N. C., Kelly, S. M., Monk, C. R., Weinberg, C. S., Oudshoorn, M. L., and Lee, C. K.: The molecular basis of the effect of temperature on enzyme activity, Biochem. J., 425, 353–360, https://doi.org/10.1042/BJ20091254, 2010.

675   Endres, S. C., Sandrock, C., Focke, W. W.: A simplicial homology algorithm for Lipschitz optimisation, J. Global Optim., 72, 181-217, https://doi.org/10.1007/s10898-018-0645-y, 2018.

Enting, I. G., Trudinger, C. M., Francey, R. J., and Granek, H.: Synthesis inversion of atmospheric CO_2 using the GISS tracer transport model, Tech. Rep. 29, Division of Atmospheric Research Technical Paper, CSIRO, Australia, available at: http: //www.cmar.csiro.au/e-print/open/enting_1993a.pdf, 1993.

680   Evans, J. R., Caemmerer, S. V, Setchell, B. A., and Hudson, G. S.: The relationship between CO2 transfer conductance and leaf anatomy in transgenic tobacco with a reduced content of Rubisco, Funct. Plant Biol., 21(4), 475–495, https://doi.org/10.1071/PP9940475, 1994.

Gelaro, R., McCarty, W., Suárez, M. J., Todling, R., Molod, A., Takacs, L., Randles, C. A., Darmenov, A., Bosilovich, M. G., Reichle, R., Wargan, K., Coy, L., Cullather, R., Draper, C., Akella, S., Buchard, V., Conaty, A., da Silva, A. M., Gu, W., Kim,
685   G.-K., Koster, R., Lucchesi, R., Merkova, D., Nielsen, J. E., Partyka, G., Pawson, S., Putman, W., Rienecker, M., Schubert, S. D., Sienkiewicz, M., and Zhao, B.: The Modern-Era Retrospective Analysis for Research and Applications, Version 2 (MERRA-2), J. Clim., 30(14), 5419–5454, https://doi.org/10.1175/JCLI-D-16-0758.1, 2017.

Glatthor, N., Höpfner, M., Baker, I. T., Berry, J., Campbell, J. E., Kawa, S. R., Krysztofiak, G., Leyser, A., Sinnhuber, B. M., Stiller, G. P., Stinecipher, J., and Von Clarmann, T.: Tropical sources and sinks of carbonyl sulfide observed from space,
690   Geophys. Res. Lett., 42(22), 10082–10090, https://doi.org/10.1002/2015GL066293, 2015.

Haynes, K., Baker, I., and Denning, S.: Simple Biosphere Model version 4.2 (SiB4) technical description, Mountain Scholar, 730 Colorado State University, Fort Collins, CO, USA. [online] Available at: https://hdl.handle.net/10217/200691., 2020.

Kattge, J., Knorr, W., Raddatz, T., and Wirth, C.: Quantifying photosynthetic capacity and its relationship to leaf nitrogen content for global-scale terrestrial biosphere models, Glob. Change Biol., 15, 976–991, https://doi.org/10.1111/j.1365-
695   2486.2008.01744.x, 2009.

Haynes, K. D., Baker, I. T., Denning, A. S., Stöckli, R., Schaefer, K., Lokupitiya, E. Y., and Haynes, J. M.: Representing grasslands using dynamic prognostic phenology based on biological growth stages: 1. Implementation in the Simple Biosphere Model (SiB4), J. Adv. Model. Earth Syst., 11(12), 4423–4439, https://doi.org/10.1029/2018MS001540, 2019.

Kesselmeier, J., Teusch, N., and Kuhn, U.: Controlling variables for the uptake of atmospheric carbonyl sulfide by soil, J.
700   Geophys. Res., 104, 11577–11584, https://doi.org/10.1029/1999JD900090, 1999.

Kettle, A. J., Kuhn, U., von Hobe, M., Kesselmeier, J., and Andreae, M. O.: Global budget of atmospheric carbonyl sulfide: Temporal and spatial variations of the dominant sources and sinks, J. Geophys. Res.-Atmos., 107, 4658, https://doi.org/10.1029/2002JD002187, 2002.

Kohonen, K.-M., Kolari, P., Kooijmans, L. M. J., Chen, H., Seibt, U., Sun, W., and Mammarella, I.: Towards standardized
705   processing of eddy covariance flux measurements of carbonyl sulfide, Atmos. Meas. Tech., 13(7), 3957–3975, https://doi.org/10.5194/amt-13-3957-2020, 2020.

Kooijmans, L. M. J., Uitslag, N. A. M., Zahniser, M. S., Nelson, D. D., Montzka, S. A., and Chen, H.: Continuous and high-precision atmospheric concentration measurements of COS, CO_2, CO and H_2O using a quantum cascade laser spectrometer (QCLS), Atmos. Meas. Tech., 9, 5293-5314, https://doi.org/10.5194/amt-9-5293-2016, 2016.

710   Kooijmans, L. M. J., Maseyk, K., Seibt, U., Sun, W., Vesala, T., Mammarella, I., Kolari, P., Aalto, J., Franchin, A., Vecchi, R., Valli, G., and Chen, H.: Canopy uptake dominates nighttime carbonyl sulfide fluxes in a boreal forest, Atmos. Chem. Phys., 17, 11453–11465, https://doi.org/10.5194/acp-17-11453-2017, 2017.

Kooijmans, L. M. J., Sun, W., Aalto, J., Erkkilä, K.-M. M., Maseyk, K., Seibt, U., Vesala, T., Mammarella, I., and Chen, H.: Influences of light and humidity on carbonyl sulfide-based estimates of photosynthesis, Proc. Natl. Acad. Sci. U. S. A., 116(7),

715   2470–2475, https://doi.org/10.1073/pnas.1807600116, 2019.

Kooijmans, L. M. J., Cho, A., Ma, J., Kaushik, A., Haynes, K. D., Baker, I., Luijkx, I. T., Groenink, M., Peters, W., Miller, J. B., Berry, J. A., Ogée, J., Meredith, L. K., Sun, W., Kohonen, K.-M., Vesala, T., Mammarella, I., Chen, H., Spielmann, F. M., Wohlfahrt, G., Berkelhammer, M., Whelan, M. E., Maseyk, K., Seibt, U., Commane, R., Wehr, R., and Krol, M.: Evaluation of carbonyl sulfide biosphere exchange in the Simple Biosphere Model (SiB4), Biogeosciences, 18, 6547–6565,

720   https://doi.org/10.5194/bg-18-6547-2021, 2021.

Kuai, L., Worden, J. R., Campbell, J. E., Kulawik, S. S., Li, K.-F. F., Lee, M., Weidner, R. J., Montzka, S. A., Moore, F. L., Berry, J. A., Baker, I., Denning, A. S., Bian, H., Bowman, K. W., Liu, J., and Yung, Y. L.: Estimate of carbonyl sulfide tropical oceanic surface fluxes using aura tropospheric emission spectrometer observations, J. Geophys. Res., 120(20), 11,11-12,23, https://doi.org/10.1002/2015JD023493, 2015.

725   Lai, C. T., Katul, G., Oren, R., Ellsworth, D., and Schäfer, K.: Modeling CO2 and water vapor turbulent flux distributions within a forest canopy, J. Geophys. Res-Atmos., 105, 26333–26351, https://doi.org/ 10.1029/2000JD900468, 2000.

Launiainen, S., Katul, G. G., Kolari, P., Vesala, T., and Hari, P.: Empirical and optimal stomatal controls on leaf and ecosystem level CO2 and H2O exchange rates, Agr. Forest Meteorol., 151, 1672–1689, https://doi.org/10.1016/j.agrformet.2011.07.001, 2011.

730   Launois, T., Belviso, S., Bopp, L., Fichot, C. G., and Peylin, P.: A new model for the global biogeochemical cycle of carbonyl sulfide – Part 1: Assessment of direct marine emissions with an oceanic general circulation and biogeochemistry model, Atmos. Chem. Phys., 15(5), 2295–2312, https://doi.org/10.5194/acp-15-2295-2015, 2015.

Lee, C. K., Daniel, R. M., Shepherd, C., Saul, D., Cary, S. C., Danson, M. J., Eisenthal, R., and Peterson, M. E.: Eurythermalism and the temperature dependence of enzyme activity. FASEB J. 21, 1934-1941, https://doi.org/ 10.1096/fj.06-

735   7265com, 2007.

Leuning, R., Dunin, F. X., and Wang, Y. -P.: A two-leaf model for canopy conductance, photosynthesis and partitioning of available energy. II. Comparison with measurements, Agr. Forest Meteorol., 91, 113-125, https://doi.org/10.1016/S0168-1923(98)00074-4, 1998.

Lombardozzi, D. L., Zeppel, M. J. B., Fisher, R. A., and Tawfik, A.: Representing nighttime and minimum conductance in

740   CLM4.5: global hydrology and carbon sensitivity analysis using observational constraints, Geosci. Model Dev., 10(1), 321–331, https://doi.org/10.5194/gmd-10-321-2017, 2017.

Ma, J., Kooijmans, L. M. J., Cho, A., Montzka, S. A., Glatthor, N., Worden, J. R., Kuai, L., Atlas, E. L., and Krol, M. C.: Inverse modelling of carbonyl sulfide: implementation, evaluation and implications for the global budget, Atmos. Chem. Phys., 21, 3507–3529, https://doi.org/10.5194/acp-21-3507-2021, 2021.

745   Maignan, F., Abadie, C., Remaud, M., Kooiijmans, L. M. J., Kohonen, K.-M., Commane, R., Wehr, R., Campbell, J. E., Belviso, S., Montzka, S. A., Raoult, N., Seibt, U., Shiga, Y. P., Vuichard, N., Whelan, M. E., and Peylin, P.: Carbonyl sulfide:

comparing a mechanistic representation of the vegetation uptake in a land surface model and the leaf relative uptake approach, Biogeosciences, 18(9), 2917–2955, https://doi.org/10.5194/bg-18-2917-2021, 2021.

Maseyk, K., Berry, J. A., Billesbach, D., Campbell, J. E., Torn, M. S., Zahniser, M., and Seibt, U.: Sources and sinks of
750 carbonyl sulfide in an agricultural field in the Southern Great Plains, P. Natl. Acad. Sci. USA, 111(25), 9064–9069, https://doi.org/10.1073/pnas.1319132111, 2014.

Michaelis, L., Menten, M. L.: Kinetik der Invertinwirkung, Biochem. Zeitung, 49, 333-369, 1913.

Miner, G. L., Bauerle, W. L., and Baldocchi, D. S.: Estimating the sensitivity of stomatal conductance to photosynthesis: a review, Plant Cell Environ., 40, 1214-1238. https://doi.org/10.1111/pce.12861, 2017.

755 Ogée, J., Sauze, J., Kesselmeier, J., Genty, B., Van Diest, H., Launois, T., and Wingate, L.: A new mechanistic framework to predict OCS fluxes from soils, Biogeosciences, 13(8), 2221–2240, https://doi.org/10.5194/bg-13-2221-2016, 2016.

Papale, D., Reichstein, M., Aubinet, M., Canfora, E., Bernhofer, C., Kutsch, W., Longdoz, B., Rambal, S., Valentini, R., Vesala, T., and Yakir, D.: Towards a standardized processing of Net Ecosystem Exchange measured with eddy covariance technique: algorithms and uncertainty estimation, Biogeosciences, 3, 571–583, https://doi.org/10.5194/bg-3-571-2006, 2006.

760 Peterson, M. E., Eisenthal, R., Danson, M. J., Spence, A., and Daniel, R. M.: A new intrinsic thermal parameter for enzymes reveals true temperature optima, J. Biological Chem., 279, 20717– 20722, https://doi.org/10.1074/jbc.M309143200, 2004.

Protoschill-Krebs, G., Wilhelm, C., and Kesselmeier, J.: Consumption of carbonyl sulphide (COS) by higher plant carbonic anhydrase (CA), Atmos. Environ., 30, 3151–3156, https://doi.org/10.1016/1352-2310(96)00026-X, 1996.

Remaud, M., Chevallier, F., Maignan, F., Belviso, S., Berchet, A., Parouffe, A., Abadie, C., Bacour, C., Lennartz, S., and
765 Peylin, P.: Plant gross primary production, plant respiration and carbonyl sulfide emissions over the globe inferred by atmospheric inverse modelling, Atmos. Chem. Phys., 22, 2525–2552, https://doi.org/10.5194/acp-22-2525-2022, 2022.

Sato, N., Sellers, P. J., Randall, D. A., Schneider, E. K., Shukla, J., Kinter III, J. L., Hou, Y.-T., and Albertazzi, E.: Effects of implementing the Simple Biosphere Model in a general circulation model. J. Atmos. Sci., 46(18), 2757-2782, https://doi.org/10.1175/1520-0469(1989)046<2757:EOITSB>2.0.CO;2, 1989.

770 Seibt, U., Kesselmeier, J., Sandoval-Soto, L., Kuhn, U., and Berry, J. A.: A kinetic analysis of leaf uptake of COS and its relation to transpiration, photosynthesis and carbon isotope fractionation, Biogeosciences, 7(1), 333–341, https://doi.org/10.5194/bg-7-333-2010, 2010.

Sellers, P. J., Mintz, Y., Sud, Y. C., and Dalcher, A.: A Simple Biosphere Model (SiB) for use within general circulation models. J. Atmos. Sci, 43(6), 505-531, https://doi.org/10.1175/1520-0469(1986)043<0505:ASBMFU>2.0.CO;2, 1986.

775 Sellers, P. J., Randall, D. A., Collatz, G.J., Berry, J. A., Field, C. B., Dazlich, D. A., Zhang, C., Collelo, G. D., and Bounoua, L.: A revised land surface parameterization (SiB2) for atmospheric GCMs. Part I: Model Formulation. J. Climate, 9(4), 676-705, https://doi.org/10.1175/1520-0442(1996)009<0676:ARLSPF>2.0.CO;2, 1996.

Smith, N. E., Kooijmans, L. M. J., Koren, G., van Schaik, E., van der Woude, A. M., Wanders, N., Ramonet, M., XuerefRemy, I., Siebicke, L., Manca, G., Brümmer, C., Baker, I. T., Haynes, K. D., Luijkx, I. T., and Peters, W.: Spring enhancement

780 and summer reduction in carbon uptake during the 2018 drought in northwestern Europe, Philos. T. Roy. Soc. B, 375, 20190509, https://doi.org/10.1098/rstb.2019.0509, 2020.

Stimler, K., Montzka, S. A., Berry, J. A., Rudich, Y., and Yakir, D.: Relationships between carbonyl sulfide (COS) and CO2 during leaf gas exchange, New Phytol., 186(4), 869–878, https://doi.org/10.1111/j.1469-8137.2010.03218.x, 2010.

Stimler, K., Berry, J. A., Montzka, S. A., and Yakir, D.: Association between carbonyl sulfide uptake and 18delta during gas
785 exchange in C3 and C4 leaves, Plant Physiol., 157(1), 509–517, https://doi.org/10.1104/pp.111.176578, 2011.

Stimler, K., Berry, J. A., and Yakir, D.: Effects of carbonyl sulfide and carbonic anhydrase on stomatal conductance, Plant Physiol., 158(1), 524-530, https://doi.org/10.1104/pp.111.185926, 2012.

Sun, W., Maseyk, K., Lett, C., and Seibt, U.: A soil diffusion--reaction model for surface COS flux: COSSM v1, Geosci. Model Dev., 8(10), 3055–3070, https://doi.org/10.5194/gmd-8-3055-2015, 2015.

790 Sun, W., Kooijmans, L. M. J., Maseyk, K., Chen, H., Mammarella, I., Vesala, T., Levula, J., Keskinen, H., and Seibt, U.: Soil fluxes of carbonyl sulfide (COS), carbon monoxide, and carbon dioxide in a boreal forest in southern Finland, Atmos. Chem. Phys., 18, 1363–1378, https://doi.org/10.5194/acp-18-1363-2018, 2018.

Tarantola, A. and Valette, B.: Inverse problems = Quest for information, J. Geogr, 50, 159-170, 1982.

Vesala, T., Kohonen, K.-M., Kooijmans, L. M. J., Praplan, A. P., Foltýnová, L., Kolari, P., Kulmala, M., Bäck, J., Nelson, D.,
795 Yakir, D., Zahniser, M., and Mammarella, I.: Long-term fluxes of carbonyl sulfide and their seasonality and interannual variability in a boreal forest, Atmos. Chem. Phys., 22, 2569–2584, https://doi.org/10.5194/acp-22-2569-2022, 2022.

Walker, A. P., Beckerman, A. P., Gu, L., Kattge, J., Cernusak, L. A., Domingues, T. F., and Woodward, F. I.: The relationship of leaf photosynthetic traits–Vcmax and Jmax–to leaf nitrogen, leaf phosphorus, and specific leaf area: A meta-analysis and modeling study, Ecol. Evol., 4, 3218–3235, https://doi.org/10.1002/ece3.1173, 2014.

800 Wehr, R, J.W. Munger, D.D. Nelson, J.B. McManus, M.S. Zahniser, S.C. Wofsy, and S.R. Saleska.: Long-term eddy covariance measurements of the isotopic composition of the ecosystem–atmosphere exchange of CO2 in a temperate forest., Agr. Forest Meteorol., 181, 69-84, https://doi.org/10.1016/j.agrformet.2013.07.002, 2013.

Wehr, R. and Saleska, S. R.: An improved isotopic method for partitioning net ecosystem–atmosphere CO2 exchange, Agr. Forest Meteorol., 214–215, 515–531, https://doi.org/10.1016/j.agrformet.2015.09.009, 2015.

805 Wehr, R, J.W. Munger, J.B. McManus, D.D. Nelson, M.S. Zahniser, Eric A Davidson, S.C. Wofsy, and S.R. Saleska.: Seasonality of temperate forest photosynthesis and daytime respiration, Nature, 534(7609), 680–83, https://doi.org/10.1038/nature17966, 2016.

Wehr, R., Commane, R., Munger, J. W., McManus, J. B., Nelson, D. D., Zahniser, M. S., Saleska, S. R., and Wofsy, S. C.: Dynamics of canopy stomatal conductance, transpiration, and evaporation in a temperate deciduous forest, validated by
810 carbonyl sulfide uptake, Biogeosciences, 14(2), 389–401, https://doi.org/10.5194/bg-14-389-2017, 2017.

Wehr, R. and Saleska, S. R.: Calculating canopy stomatal conductance from eddy covariance measurements, in light of the energy budget closure problem, Biogeosciences, 18, 13–24, https://doi.org/10.5194/bg-18-13-2021, 2021.

Whelan, M. E., Lennartz, S. T., Gimeno, T. E., Wehr, R., Wohlfahrt, G., Wang, Y., Kooijmans, L. M. J., Hilton, T. W., Belviso, S., Peylin, P., Commane, R., Sun, W., Chen, H., Kuai, L., Mammarella, I., Maseyk, K., Berkelhammer, M., Li, K.-., Yakir,

815   D., Zumkehr, A., Katayama, Y., Ogée, J., Spielmann, F. M., Kitz, F., Rastogi, B., Kesselmeier, J., Marshall, J., Erkkilä, K.-., Wingate, L., Meredith, L. K., He, W., Bunk, R., Launois, T., Vesala, T., Schmidt, J. A., Fichot, C. G., Seibt, U., Saleska, S., Saltzman, E. S., Montzka, S. A., Berry, J. A., and Campbell, J. E.: Reviews and syntheses: Carbonyl sulfide as a multi-scale tracer for carbon and water cycles., Biogeosciences, 15, 3625–3657, https://doi.org/10.5194/bg-15-3625-2018, 2018.

White, M. L., Zhou, Y., Russo, R. S., Mao, H., Talbot, R., Varner, R. K., and Sive, B. C.: Carbonyl sulfide exchange in a
820   temperate loblolly pine forest grown under ambient and elevated CO2, Atmos. Chem. Phys., 10, 547–561, https://doi.org/10.5194/acp10-547-2010, 2010.

Wolf, A., Akshalov, K., Saliendra, N., Johnson, D. A., and Laca, E. A.: Inverse estimation of Vcmax, leaf area index, and the Ball–Berry parameter from carbon and energy fluxes, J. Geophys. Res-Atmos., 111, https://doi.org/ 10.1029/2005JD005927, 2006.

825   Woodward, F. I., Smith, T. M., and Emanuel, W. R.: A global land primary productivity and phytogeography model. Global Biogeochem. Cy., 9, 471–490, https://doi.org/10.1029/95GB02432, 1995.